# Distance Maps and Plant Development #2: Facilitated Transport and Uniform Gradient

Pavel Dimitrov and Steven W. Zucker

May 28, 2009

**Abstract**

The principles underlying plant development are extended to allow a more molecular mechanism to elaborate the schema by which ground cells differentiate into vascular cells. Biophysical considerations dictate that linear dynamics are not sufficent to capture facilitated auxin transport (e.g., through PIN). We group these transport facilitators into a non-linear model under the assumption that they attempt to minimize certain *differences* of auxin concentration. This Constant Gradient Hypothesis greatly increases the descriptive power of our model to include complex dynamical behaviour. Specifically, we show how the early pattern of PIN1 expression appears in the embryo, how the leaf primordium emerges, how convergence points arise on the leaf margin, how the first loop is formed, and how the intricate pattern of PIN shifts during the early establishment of vein patterns in incipient leaves of Arabidopsis. Given our results, we submit that the model provides evidence that many of the salient structural characteristics that have been described at various stages of plant development can arise from the uniform application of a small number of abstract principles.

## Contents

# 1 Introduction

In the companion paper [14] we introduced a model for auxin dynamics that can predict key features of leaf vein patterns. While it is remarkable that diffusion of the hormone provides a sufficient basis to describe these patterns, this transport mechanism does not accurately describe the flow of auxin in plants. Facilitated transport of the hormone has been postulated since the proposal of the chemiosmotic theory, and recent molecular genetic and cell biological findings support this theory. Genes and related proteins have recently been identified as either influx (e.g., AUX) or efflux (e.g., PIN) auxin 'carriers'. Most interestingly, the experiments suggest that the hormone may in fact be 'pushed' against a concentration gradient — that is, opposite to the direction of diffusion flow in the sense of our earlier model. The carriers also appear to increase flow in the direction of diffusion flow at times, but why this dual function exists and when it shifts from one to the other is not well understood. Opinion among experimentalists is split, resulting in a conundrum for plant developmental biology. Recent experiments that focus on facilitated transport due to the PIN1 gene provide another dimension to the conundrum. Scarpella *et al.* [51] visualize PIN1 expression domain, or PED, at different stages of early leaf development and observe that eventually the PED defines the vein pattern exactly. Curiously, the PED undergoes several transformations whereby certain parts appear temporarily only to disappear just before the final pattern is established. Yet, the patterns that the PED defines are robust to cell divisions. The dynamics are non-linear and sometimes counter-intuitive. It would appear, therefore, that a carefully timed complex genetic machinery must exist for the purpose of controlling these events.

Contrary to this intuition, in this paper we demonstrate that the underlying principles that guide such intricate events need not be many. While our focus remains abstract, our goal is to bring our model closer to cell and molecular biology. We concentrate on the phenomenon of polar transport rather than its molecular implementation and extend our earlier model to accommodate this abstraction. Building on the two principles from our earlier work, the Constant Production Hypothesis and the Proportional Destruction Hypothesis, we develop the Constant Gradient Hypothesis, which we use to derive a new computational tool to test the theoretical predictions. We introduce a non-linear model mathematically and then use it to analyze the observations reported by Scarpella *et al.* [51]. We focus on the shifting patterns of the PED during early leaf development, and discuss schematic simulations to offer an explanation for key stages of those events. Thus we illustrate how our theory captures certain intricate patterning events. Insofar as the polar

Figure 1: Sketch of predictions.

| Protein | Polar Membrane Localization | Auxin "carrier" | References |
|---|---|---|---|
| PIN1 | Yes | Efflux | [39], [22] |
| PIN2 | Yes | Efflux | [12], [32], [34], [57], [54], [1], [8] |
| PIN3 | – | Efflux | [21] |
| PIN4 | Yes | Efflux | [18], [48] |
| PIN7 | – | Efflux | [20] |
| MDR1/ PGP{1,2,4,19} | Yes and No | Efflux | [10], [24], [35], [36], [38], [37] |
| AUX1 | Yes | Influx | [6], [55], [2] |

Table 1: The variety of auxin facilitators reveals enormous potential for complex interactions. Since many of these remain to be studied, we study their net effect.

transport mechanism is implemented by a single substance, our simulations predict the behavior of that substance; however, (and this is key) our polar transport extension is meant as a simplifying abstraction of the Chemiosmotic Theory that captures the total effect of various substances acting together, rather than the behavior of any one substance. To preview the scope of our predictions, we sketch in Fig. 1 certain of the pivotal events in vascular development. Once our theory is developed, we return to these predictions via simulation.

## 2 Auxin Transport

Auxin travels through plants by moving between cells. It may leave a cell interior, the cytoplasm, pass through the plasmalemma and then reach the cell walls, or apoplast. It can then move into the cytoplasm of an adjacent cell and continue diffusing in this fashion throughout the plant. Perhaps the first real breakthrough in understanding how this movement occurs was the introduction of the chemiosmotic theory in the 1970s. Based only on physical chemistry and a handful of measurements, Rubery and Sheldrake [46, 47] and Raven [44] were able to predict that auxin cannot travel by diffusion alone; that some sort of active transport (i.e. one that requires energy expenditure) must be present; and that some sort of carrier substances must exist that move auxin in a preferred direction—toward the cytoplasm (influx) or away from it (efflux).

It is "remarkable how accurately [this] molecular model [...] fits with the recent molecular genetic and cell biological findings" [58]. Increasingly, the evidence suggests that auxin transport is facilitated in both directions. The AUX proteins are a family of putative influx carriers [2, 56, 13, 60, 30], while the PIN family [30, 58] and the multidrug resistance/p-glyvoprotein (MDR/PGP) family of proteins [7] are thought to be efflux carriers. Recent molecular techniques, which can

effectively 'color' specific molecules with sub-cellular precision [19], have shown that both types of facilitators may localize asymmetrically on the plasmalemma although MDR/PGP proteins do not always do that [50]. Indeed, many proteins have been implicated in auxin transport, as Table 1 summarizes, and often more than one substance is present in the same cell at the same time. It is therefore difficult to infer the pattern of auxin transport from this detailed mechanistic view of auxin transport.

In order to analyze how the patterns of auxin transport form we shall consider polar transport in a cell as the total effect of polar transport as predicted by the chemiosmotic theory. So, for example, if both AUX proteins and PIN proteins are expressed in a cell in equal measure and on the same parts of the membrane, then the action of the influx carriers will be canceled by the action of the efflux carriers and the total effect will be nil. Conversely, if we observe a total efflux effect in a given cell, then this only implies that the balance between influx and efflux carriers favors the latter. This simplification requires a refinement to our earlier model, which we prove to be consistent with the Chemiosmotic theory in Appendix A. In particular, we may limit the analysis to the movement of auxin between cell interiors and yet capture a sufficiently accurate picture of the whole process. We note that, if the molecular carriers in a given region of cell are always of the same kind, as seems to be the case in Scarpella *et al.* [51] (all PIN1), then any predictions using this simplification apply directly to that carrier. For this reason and because most of the experiments that we shall analyze involve only PIN proteins, we shall refer to our simplification of directed (polar) transport as "PIN" transport.

The key difference between the model that we develop here and our earlier formulation is that polar transport may move auxin against concentration gradients (from low to high concentrations) and therefore counteract the passive diffusion flow. The modeling challenge thus moves beyond that of Fickian diffusion, but its importance increases dramatically. The reward is that the capability for pattern formation is enlarged as well. We now explore this increased capability.

## 3 "PIN" Polarity

We now consider some of the experimental evidence concerning PIN1. This will be the basis for our assumptions about polar transport recognizing the fact that the experiments reviewed below show PIN1 but other carriers may be present in the same cells.

## 3.1 A Conundrum

The appearance of PIN1 in detectable quantities is intimately related to auxin [59, 41], but the polarity of the carrier need not follow the diffusive auxin flow. For example, Reinhardt *et al.* [45] report that the pattern of PIN expression changes after a micro-application of auxin in shoot meristems—the polar transport acts toward the application site. In leaves, on the other hand, Scarpella *et al.* [52] applied the hormone to a small portion of a developing primordium and noticed that PIN1 oriented so that the hormone would be better drained away from the leaf, i.e. away from the application site. The application site in both cases has a higher auxin concentration than the rest of the organ so, considering each experiment separately, two mechanisms come to mind:

MECHANISM 1: New PIN1 appears at a membrane against diffusion flow when this flow, or difference of concentration, is large enough.

MECHANISM 2: New PIN1 appears at a membrane 'helping' diffusion flow.

At first glance it looks like neither rule can explain both experiments because the phenomena appear to be mutually exclusive. But it turns out that one of these schematic mechanisms is the foundation of a model that predicts both phenomena in detail as well as vein patterns and the growth of organs more generally.

## 3.2 PIN1 Polarity Under Cell Division

Our first clue comes from considering what happens when a cell with PIN1 expression divides. In leaf primordia, the cells that will eventually become part of the midvein are marked by PIN1 expression that localizes toward the base of the cell, i.e. toward the stem and away from the leaf tip. This pattern appears as soon as the primordium emerges from the shoot apical meristem and the polarity of the cells is maintained even during frequent cell divisions. When a cell with PIN1 expression divides perpendicularly to the midvein strand, a new membrane is created that also acquires PIN1 expression with the polarity of the original cell. Mechanism 1 fails to predict such behavior, while Mechanism 2 maintains the proper PIN1 polarity. We reason as follows.

Consider the illustration in Fig. 2*A–D*. Initially, the concentration of auxin in the middle cells is higher than in the cell on the left and lower than in the cell on the right. When the middle cell divides its membrane is 'split' and a new barrier forms. The existing auxin carriers then drain auxin away from the daughter compartment on the right and push auxin into the neighbor cell on the

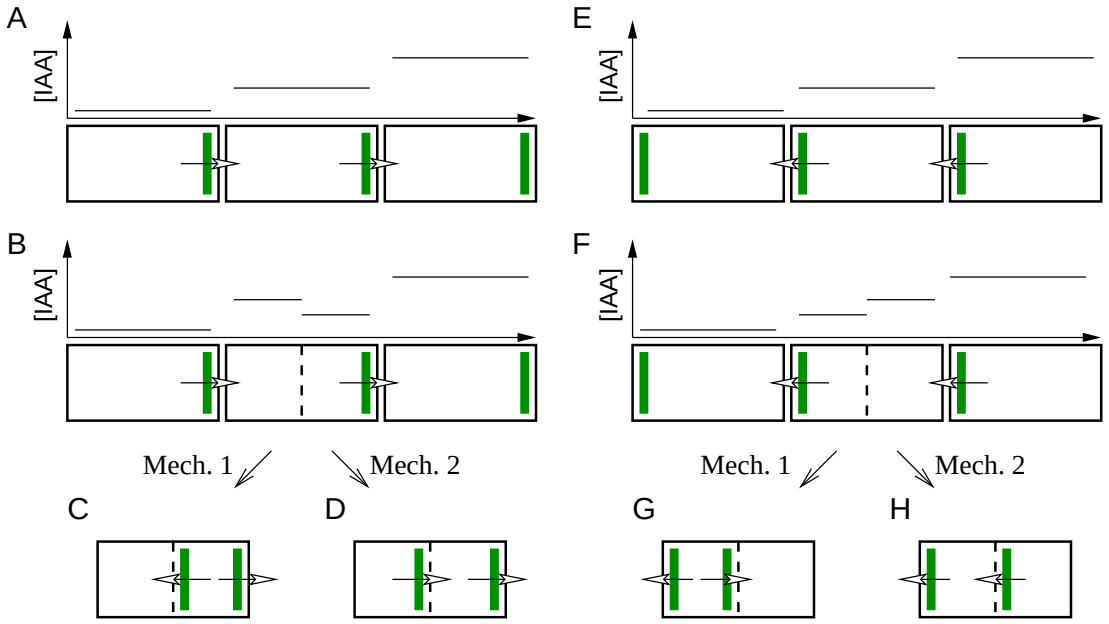


Figure 2: Illustration of the effect of two presumptive mechanisms for PIN1 creation in the context of a cell division. Three cells are shown in *A* and *E* with consistent polarities indicated by open arrows. When the middle cell divides, its membrane remains the same except for the new membrane that splits the cell in two daughter compartments. We take this to imply that the existing PIN structure is maintained and the problem is to determine how PIN is established along the new section of membrane. The concentration of auxin (denoted [IAA]) is plotted above the depiction of each cell. PIN1, shown in green, is created according to one of two mechanisms: (1) toward higher concentrations (see *C* and *G*), or (2) toward lower concentrations (see *D* and *H*). Note that Mechanism 1 breaks the continuity of PIN polarity in both cases, whereas Mechanism 2 maintains this continuity. **(A–D)** PIN1 acts against diffusive flow, toward increasing concentration, e.g. as in the *Arabidopsis* root tip. **(E–H)** PIN1 'helps' diffusive flow, e.g. as in leaf primordia. **(A,E)** Configuration before cell division. **(B,F)** Configuration during cell division (dashed line) but before PIN1 is established at the new interface. **(C,D,G,H)** Configuration in middle cell (and respective daughter cells) after PIN1 is created according to Mechanism 1 (*C,G*) or Mechanism 2 (*D,H*).

left. On the other hand, the carriers from within the neighbor cell on the left push auxin into the daughter compartment on the left. Thus, the left compartment acquires a higher concentration than the right compartment. If PIN1 were to be created toward a higher concentration—Mechanism 1 and Fig. 2*C*—then it should form in the right compartment thereby creating a bipolar cell. This would be the outcome after most cell divisions and, in particular, in the midvein strand where no bipolar cells have been found. By contrast, if PIN1 were to be created predominantly toward lower concentrations of auxin—Mechanism 2 and Fig. 2*D*—then the continuity would be maintained. We therefore conclude that the first appearance of PIN1 in cells is most likely due to Mechanism 2.

Recall Schema 1 from [14] which postulates that a ground cell becomes c-vascular whenever it measures a sufficiently large $\Delta c$. At the schema level of abstraction, the change is realized as an

increased diffusion coefficient through the relevant interface, and the $\Delta c$ there decreases. This is precisely the effect of Mechanism 2! In other words, we have now shown that Schema 1 can be implemented by auxin carriers. Therefore our derivation of Schema 1 informs the appearance of auxin carriers as a result of organ geometry and cell size distribution. The agreement between these predictions and experimental fact reinforces confidence that Schema 1 is implemented by these carriers.

# 4 The Constant Gradient Hypothesis

Even though Mechanism 2 will be a useful guideline to understand PIN1 dynamics, it does not explain how the carrier concentration at the cell membrane is maintained. Indeed, the protein cycles between the interior of the cell and the plasmalemma [41], and it is somehow destroyed during the early stages of leaf development [52] and when it undergoes reorientation [45]. Moreover, even if the first appearance of PIN1 is in the direction of decreasing auxin concentration, there is carrier presence against the auxin gradient. For example, the polarity of provascular cells near the distal tip of the *Arabidopsis* root is toward the tip, and the auxin concentration increases in the same direction [30]. This suggests that the mechanism responsible for PIN1 density at the plasmalemma exhibits some sort of hysteresis memory. Taken together, the cycling, the plasticity of expression, and the memory properties of PIN1 imply that the mechanism is a dynamical system governed by a differential equation.

Mathematical formulations of this sort are common and find many applications in biology [43]. For example, they are the theoretical basis for genetic switches [3] where the equations can be understood in terms of two competing processes: the activity of promoters described by a production function, and the activity of inhibitors and natural degradation described by a destruction function. The production function depends on the concentration of the gene product whenever the product promotes the expression of the gene, and it can usually be described by a Hill function. If there are several promoter sites and cooperation between them, then the Hill coefficient is large [25, 23, 33, 17]. On the other hand, the destruction is a linear function of concentration whenever no inhibitors exist and only natural degradation depletes the substance. Configurations of this kind exhibit the behavior of a switch: if an external event lowers the concentration below a threshold $\tau$, then the system maintains the concentration at level $A$; if another external event pushes the concentration above this threshold then the system maintains the concentration at level $B$ ($B > \tau > A$). If $A$ is

biologically negligible (insufficient for additional reactions) but $B$ is not, then we can say that the gene is turned 'off' or 'on' depending on whether the product concentration is below or above the threshold, respectively.

There is more direct and independent support for the dynamics of PIN1 to be well described by a Hill function and by the concept of cooperation. Cooperation is central in the empirically derived Canalization Hypothesis by Sachs [49] whereby "flux begets flux." If the increase in flux is the result of "PIN", then the carriers must exhibit an autocatalytic behavior because they are saturable: they have a maximum capacity for transporting auxin through the plasmalemma [42, 58]. Note, however, that we are referring to the net effect and that the actual behavior may involve more than a single substance. For example, it may be the result of mutual cooperation between the PIN proteins and the MDR/PGP proteins [37, 42]. Therefore to increase the flux of auxin due to those facilitators, the concentration of the molecule must be increased. We submit the following hypothesis:

**Hypothesis 1** (PIN1 Cooperation)**.** *PIN carriers at the plasmalemma attract additional PIN carriers near them. The protein leaves the membrane when it has transported its load of auxin.*

In other words, the density of PIN carriers at a patch of the cell plasma membrane is determined by a dynamical system with a production function that depends on that density, a Hill function. The destruction function also depends on the density but can be assumed to be linear, because only a portion of the loaded proteins—those immediately adjacent to the membrane, those attached to it—can facilitate hormone transport at any given time. In effect, this configuration constitutes an auxin carrier 'switch.'

As we argued above, the external events that turn the switch 'on' or 'off' depend on auxin and, particularly, on the difference of auxin concentration $\Delta c$ through an interface. The rule which we called Mechanism 2 above implies that a large $\Delta c$ in the direction of diffusion—i.e. a positive $\Delta c$—should increase the production function. On the other hand, the reorientation of the carrier following external application of auxin implies that a high gradient against the action of PIN should increase the destruction function. Yet, the strong expression of PIN1 against the auxin gradient in provascular cells of the root tip implies that the destruction function overwhelms the production function only when $\Delta c$ is sufficiently negative. We therefore submit that PIN dynamics are modified by auxin in the following fashion:[1]

[1] In fact, a more mechanistic hypothesis that justifies Hypothesis 2 can be made. It is about both influx (e.g., AUX) and efflux (e.g., PIN) carriers and requires them to function in a dual fashion: $\Delta c$ makes it difficult for PIN to unload auxin and easy for AUX. Here, $\Delta c$ is the more immediately available difference of auxin concentration

**Hypothesis 2** (Effect of Auxin on PIN1 Dynamics)**.** *PIN accumulation on the plasmalemma is promoted by $\Delta c$ regardless of sign. The destruction function increases only when the diffusive flow opposite to the action of PIN1 increases, i.e. if the carrier pushes auxin against diffusion.*

In other words, PIN1 is more likely to be destroyed when it pushes auxin against a concentration gradient. But even in that case, the production process may still be sufficiently strong to compensate for the action of the destruction process and maintain carrier presence or, as in the root tip, even increase it. However, if the gradient is too steep, then destruction overwhelms production and carrier presence disappears.

The lack of experimental data prevents us from determining exactly when this happens and the explicit forms of the functions that describe the dynamics. This underlines the advantage of our abstraction, though: we can use our theory to infer a functional role for auxin carriers that is consistent with our hypotheses and that will allow us to predict the distribution of polar transport intensity in plants. Some data of this sort are available, and more precise measurements can be obtained with current techniques.

Recall that we required veins to possess an efficient transport mechanism for auxin. In particular, no concentration peaks should form there. On the other hand, we saw that the appearance of auxin carriers at a cell interface is most likely triggered by a high $\Delta c$ and, initially at least, helps diffusion. In effect, carriers decrease this $\Delta c$. Working against diffusion, too, they maintain a $\Delta c$ that does not exceed some fixed threshold because otherwise carrier presence would disappear. Therefore, we propose a third uniformity principle:

**Hypothesis 3** (Constant Gradient)**.** *Facilitated transport maintains the difference in auxin concentration, $\Delta c$, constant.*

# 5 Computational Model of Active Transport

The Constant Gradient Hypothesis suggests an elaboration of the computational model developed in the previous paper [14]. In this section we derive the mathematical and computational tools that are necessary to evaluate the theory. We develop a framework for simulations, which we use in the next section to illustrate how to explain experimental evidence of certain patterning phenomena.

between the cytoplasm and the cell wall instead of, as we conjecture in Hypothesis 2, a $\Delta c$ between the cytoplasms of two neighboring cells.

The tools that we develop here have a larger scope than is shown in the next section, as can be seen in the next paper [15] of this series.

## 5.1 Background

Even though auxin transport may be due to energy expenditure, the net effect may still be well described by Fick's law. This is the case when carriers are located in a non-polar fashion (homogeneously) along the cell membrane. The PGP family appears to exhibit this behavior so it can be seen as a mechanism for improving the effective diffusion coefficient. In this case, our Helmholtz formulation from [14] applies and large domains of cells can be described by the continuous equation

$$\frac{\partial c}{\partial t} = D\nabla^2 c + \frac{K}{S} - \alpha c \ . \tag{1}$$

Thinking of cells as individual compartments, this means that the concentration $c(i)$ of auxin in each cell $i$ changes as a function of time according to the transport to neighboring cells $Nbr(i)$, the production $K/S(i)$, and the destruction $-\alpha c(i)$; in symbols:

$$\frac{\partial c(i)}{\partial t} = \underbrace{\sum_{j \in Nbr(i)} D(c(j) - c(i))}_{\text{Diffusion Transport}} + \frac{K}{S(i)} - \alpha c(i) \ . \tag{2}$$

On the other hand, the PIN family of proteins (and PIN1 in particular) localize asymmetrically along the membrane—with negligible or no expression on one side of the cell and strong expression on the other. This is the scenario that we now study because it yields dynamics for auxin transport that deviates from Fick's Law: circumstances exist in which it can 'push' the hormone against concentration gradients. A typical assumption regarding the effect of transport facilitators such as PIN is that they add a linear term to the model. This turns out to be consistent with the chemiosmotic theory, as we show in Appendix A, so we incorporate this idea into our Helmholtz Model of [14] as follows:

$$\frac{\partial c(i)}{\partial t} = \underbrace{\sum_{j \in Nbr(i)} D(c(j) - c(i))}_{\text{Diffusion Transport}} + \underbrace{\sum_{j \in Nbr} p_j^{in} c(j) - \sum_{j \in Nbr} p_j^{out} c(i)}_{\text{Polar Transport}} + \frac{K}{S(i)} - \alpha c(i) \ . \tag{3}$$

Here $p_j^{in}$ is the (active) polar transport coefficient for auxin being 'pushed' into the current cell $i$

from a neighboring cell $j$, while $p_j^{out}$ is the polar transport coefficient for auxin being 'exported' from the current cell toward the neighbor $j$. Since these coefficients represent the asymmetrically located putative carrier PIN1, they also represent a measure of the work that the carrier performs. In particular, if PIN1 works at saturation, then the $p$'s are proportional to PIN1 concentration at an interface. Thus, the biological appearance of PIN1 translates into the appearance of non-zero $p$'s in this model. But how can we predict when that happens? The Constant Gradient Hypothesis offers an answer, provided that we can solve a non-linear transport problem.

## 5.2 Formulation of Non-linear Transport Problem

Suppose the cell sizes in the domain of interest (e.g., a young leaf) are known and that we also know which cells express PIN1. We are given the interfaces where the carrier is present and the direction in which it facilitates auxin transport, but we do not know how much protein is present there.[2] PIN1 may work either in the direction of diffusive flow or against it: these are two distinct modes of operation. We shall see how to assign an operation mode to each interface in the following section. Here we discuss a mathematical tool that allows us to compute the auxin concentration at equilibrium, $c$, assuming the modes of operation are known everywhere. Finally, this $c$ is used in conjunction with Eq. 3 to estimate the amount of PIN1 present at each interface.

In the first mode of operation PIN1 maintains $\Delta c < \tau_1$ because it works with diffusion. We define the following non-linear transport function:

$$\phi^{nl}(\Delta c) = \begin{cases} D & \Delta c < \tau_1 \\ D_{fast} & \Delta c \geq \tau_1 \end{cases} .$$

where $D_{fast} \gg D$. Note that the usual transport function due to Fickian diffusion is $\phi^{Fick}(\Delta c) = D\Delta c$. The only difference is that the diffusion coefficient increases non-linearly when the difference in auxin concentration through the interface exceeds the threshold $\tau_1$. The dynamics of cell $i$ become:

$$\frac{dc}{dt}(i) = \sum_{j \in Nbr(i)} \phi(c(j) - c(i)) + \frac{K}{S(i)} - \alpha c(i)$$

where $Nbr(i)$ denotes the neighboring cells of cell $i$, and the flux $\phi$ now depends on whether the interface contains PIN1 helping diffusion or not, i.e. it is either $\phi^{nl}$ or $\phi^{Fick}$. The effect of this

[2] Note that our previous model [14] can make this sort of prediction. Also, the distribution of PIN1 can be obtained from experiments such as those in [52].

formulation is that an interface with transport function (describing the flux of auxin) $\phi^{nl}$ will have a $\Delta c < \tau_1$ or $\Delta c \approx \tau_1$ at equilibrium for a sufficiently large $D_{fast}$. This is equivalent to what the Constant Gradient Hypothesis postulates for PIN1 working with diffusion.[3]

When the carrier works against the concentration gradient, however, the hypothesis implies that the $|\Delta c|$ is maintained below but near $\tau_2$. For the purposes of the present paper, this behavior can be achieved by a constant flux. For example, if PIN1 is present at the interface between cells $i$ and $j$, facilitates transport of auxin from $i$ to $j$, and $c(i) < c(j)$ (i.e. PIN1 works against diffusion), then the flux due to PIN1 is a constant $p_{uphill}$. In symbols,

$$\begin{aligned} \tfrac{dc}{dt}(i) &= \left(\textstyle\sum_{k\in Nbr(i)} \phi(c(k)-c(i)) + \frac{K}{S(i)} - \alpha c(i)\right) - p_{uphill} \\ \tfrac{dc}{dt}(j) &= \left(\textstyle\sum_{k\in Nbr(j)} \phi(c(k)-c(j)) + \frac{K}{S(j)} - \alpha c(j)\right) + p_{uphill} \end{aligned}$$

So, we only assume values for uphill polar transport and we can solve the non-linear system to obtain the distribution of auxin concentration at equilibrium (details in Section 5.3). Using this distribution we can obtain the polar transport contribution in all cells (details in Section 5.4) and obtain all the parameters of the polar transport dynamics at equilibrium (Eq. 3 with $\frac{dc}{dt} = 0$). In particular, we obtain the values of the polar transport coefficients $p^{in}$ and $p^{out}$ which are related to the density of PIN1 at the respective membranes.

The above analysis, together with our Schema 1 fleshed out as the appearance of PIN1, allows us to make much more detailed predictions. These predictions follow in Section 6 and Section 7.

## 5.3 Solving the Non-linear Dynamics Problem

Now we show how to find the equilibrium concentration of auxin according to the non-linear transport formulation. We need to find $c(i)$ for all cells $i$ that satisfies:

$$\frac{dc}{dt}(i) = \sum_{j\in Nbr(i)} \phi(c(j), c(i)) + \rho(i) - \alpha c(i) = 0 \tag{4}$$

where $Nbr(i)$ denotes the neighboring cells of cell $i$; $\phi$ is the flux of auxin from cell $j$ into cell $i$; $\rho(i) = \frac{K}{S(i)}$ is the production function; and $\alpha$ is the destruction constant. There are three types of flux functions of interest: diffusion according to Fick's Law $\phi^{Fick}$; non-linear diffusion $\phi^{nl}$; and polar transport $\phi^{polar}(c(j), c(i)) = \pm p_{uphill}$ where the sign is positive if PIN1 facilitates transport

[3]Note, however, that the non-linear dynamics do not say anything about how the system behaves outside of equilibrium. This is simply meant as tool to compute the equilibrium.

uphill from cell $j$ into cell $i$ and negative in the opposite direction. All three share properties that guarantee the dynamical system to have a unique solution.

**Proposition 1.** *Let $\phi(c(i), c(j))$ have the following properties:*

1. *Antisymmetry: $\phi(x, y) = -\phi(y, x)$*
2. *Monotonicity: $x - y \leq v - w \Longrightarrow \phi(x, y) \leq \phi(v, w)$*
3. *$\phi_x = \frac{\partial \phi}{\partial x} \geq 0$.*

*Then, there is a unique $c$ that satisfies Eq. 4 which can be found using a Newton method.*

*Proof.* Let $c$ be the distribution of concentration and define the dynamics as:

$$(c_t)(i) = \sum_{j \in Nbr(i)} \phi(c(j), c(i)) + \rho(i) - \alpha c(i) \ .$$

Now the Jacobian with respect to $c(i)$ is a matrix

$$J = \left[ \frac{\partial (c_t)(i)}{\partial c(j)} \right]_{ij}$$

with off-diagonal entries, $i \neq j$, $J_{ij} = \frac{\partial \phi(c(j), c(i))}{\partial c(j)} = \phi_x(c(j), c(i))$. The diagonal entries are

$$J_{ii} = \frac{\partial (c_t)(i)}{\partial c(i)} = \sum_{j \in Nbr(i)} \frac{\partial \phi(c(j), c(i))}{\partial c(i)} - \alpha \ = \sum_{j \in Nbr(i)} \phi_y(c(j), c(i)) - \alpha$$

where $\phi_y$ denotes the partial derivative with respect to the second argument.

Now, using the antisymmetry property, differentiating with respect to $x$ on both sides, we see that $\phi_x = -\phi_y$. Therefore, the diagonal entries of the Jacobian become

$$J_{ii} = \sum_{j \in Nbr(i)} -\phi_x(c(j), c(i)) - \alpha \ .$$

Thus, the third property implies that the diagonal entries are strictly negative and that they dominate the off-diagonal entries (because $\sum_{j \neq i} J_{ij} = \sum_{j \in Nbr(i)} \phi_x(c(j), c(i))$). As a result, the Jacobian $J$ is always invertible and Newton's method applies. In particular, this means that $J(c_t) = 0 \iff (c_t) = 0$ so such a $c$ exists because the $c > 0$ and $\sum_i c \leq \sum_i \rho/\alpha$ under these dynamics.

It is also unique. Let the transport operator $\Phi$ be defined as

$$(\Phi c)(i) = \sum_{j \in Nbr(i)} \phi(c(j), c(i))$$

and suppose that both $x$ and $y$ are solutions. Thus,

$$\Phi x - \alpha x = -\rho = \Phi y - \alpha y \Longrightarrow \Phi x - \Phi y = \alpha(x - y)$$

So the inner product

$$(\Phi x - \Phi y, x - y) = \alpha(x - y, x - y) \geq 0 \ . \tag{5}$$

On the other hand

$$(\Phi x - \Phi y, x - y) = (\Phi x, x) - (\Phi x, y) - (\Phi y, x) + (\Phi y, y) \tag{6}$$

where

$$(\Phi x, x) = \sum_i x_i (\Phi x)(i) = \sum_i x_i \left( \sum_{j \in Nbr(i)} \phi(x_j, x_i) \right) \ .$$

Each pair of neighbors appears exactly twice in the flux function: once for each direction. Thus, the term $x_i \phi(x_j, x_i)$ corresponds to the term $x_j \phi(x_i, x_j)$. Therefore, using the first property we can pair the two terms as $(x_i - x_j)\phi(x_j, x_i)$. The expression for the $(\Phi x, x)$ then becomes

$$(\Phi x, x) = \sum_{j \neq i \ Nbrs} (x_i - x_j)\phi(x_j, x_i)$$

where the sum is over all pairs of neighbors $i$ and $j$. Using the same argument, we obtain expressions for the other inner products and rewrite Eq. 6 as

$$\begin{aligned} &(\Phi x - \Phi y, x - y) \\ &\quad = \sum (x_i - x_j)\phi(x_j, x_i) - (y_i - y_j)\phi(x_j, x_i) - (x_i - x_j)\phi(y_j, y_i) + (y_i - y_j)\phi(y_j, y_i) \\ &\quad = \sum -(x_i - x_j)\phi(x_i, x_j) + (y_i - y_j)\phi(x_i, x_j) + (x_i - x_j)\phi(y_i, y_j) - (y_i - y_j)\phi(y_i, y_j) \end{aligned}$$

Let $A = x_i - x_j$, $\phi(A) = \phi(x_i, x_j)$, $B = y_i - y_j$, and $\phi(B) = \phi(y_i, y_j)$. So we can rewrite the terms

in the summation as

$$-A\phi(A) + B\phi(A) + A\phi(B) - B\phi(B) = -(A-B)(\phi(A) - \phi(B)) \ .$$

The second property of $\phi$ guarantees that $(A - B)$ and $\phi(A) - \phi(B)$ have the same sign, i.e. $-(A-B)(\phi(A) - \phi(B)) \leq 0$. Therefore, $(\Phi x - \Phi y, x - y) \leq 0$. Thus, recalling Eq. 5, we see that $(\Phi x - \Phi y, x - y) = 0$, which either means that $x = y$ and we are done, or that $\Phi x = \Phi y$. In the latter case, we have

$$\Phi x - \alpha x = \Phi y - \alpha y \Longrightarrow -\alpha x = -\alpha y \Longrightarrow x = y$$

so the solution is unique. □

## 5.4 Computing the Polar Transport Contribution

Now suppose that the distribution of auxin concentration at equilibrium, $c$, is known—e.g., computed as in Section 5.3—and that the polar transport dynamics are given by

$$\frac{dc}{dt}(i) = \sum_{j \in Nbr(i)} (D(c(j) - c(i)) - \pi_{i\to j} + \pi_{j\to i}) + \frac{K}{S(i)} - \alpha c(i) = 0 \tag{7}$$

where $\rho(i) = K/S(i)$ and $\alpha$ are also known. Our task here is to compute the effective polar transport contribution: the $\pi_{i\to j}$. The unsaturated polar transport and the effective polar transport are related

$$\pi_{i\to j} = p_{i\to j} c(i) \tag{8}$$

so we can rewrite Eq. 7 in matrix form:

$$\mathcal{D}\mathbf{c} + \mathcal{P}\mathbf{c} + \rho - \alpha\mathcal{I}\mathbf{c} = 0 \tag{9}$$

where $\mathcal{D}$ is the diffusion matrix as described in [14]; $\mathcal{P}$ is the polar transport matrix; $\rho$ is the production vector; and $\mathcal{I}$ is the identity matrix. The polar transport matrix is everywhere zero except for interfaces $i|j$ with polar transport. Thus, if the direction of transport is $i \to j$, then $\mathcal{P}_{ij} = p_{i\to j}$ and $\mathcal{P}_{ii} = -p_{i\to j} + Other$ (where $Other$ refers to other polar interfaces that cell $i$ may have). This contributes $-p_{i\to j}c(i)$ to the dynamics of cell $i$ and $p_{i\to j}c(i)$ to the dynamics of cell $j$ as required. The unknowns are the $p_{i\to j}$, i.e. the entries of $\mathcal{P}$. Let $\mathbf{p}$ be the vector of those unknowns

and write

$$(\mathcal{P}^*)\mathbf{p} = \mathcal{P}\mathbf{c} \ . \tag{10}$$

Eq. 9 implies that

$$\mathcal{P}\mathbf{c} = (-\mathcal{D} + \alpha\mathcal{I})\mathbf{c} - \rho, \tag{11}$$

which contains no unknowns and can be computed. The matrix $\mathcal{P}^*$ is the dual of $\mathcal{P}$ and can be written as follows. The $i^{th}$ coordinate of the vector $\mathcal{P}\mathbf{c}$ consists of the sum of the contribution of all outgoing polar transport activity—cell $i$ exporting to neighbors—and all incoming activity—neighbors exporting toward cell $i$.

$$[(\mathcal{P}^*)\mathbf{p}]_i = \sum_{j \in out} -p_{i\to j}c(i) + \sum_{j \in in} p_{j\to i}c(j) = [\mathcal{P}\mathbf{c}]_i \tag{12}$$

so combining with Eq. 8 we obtain an expression $\pi_{i\to j}$

$$[\Pi\vec{\pi}]_i = \sum_{j \in out} -\pi_{i\to j} + \sum_{j \in in} \pi_{j\to i} = [\mathcal{P}\mathbf{c}]_i \tag{13}$$

where $\vec{\pi}$ is the vector of effective polar transport variables, and $\Pi$ is the $n \times m$ incidence matrix for the polar transport graph where $n$ is the number of cells and $m$ is the number of edges. Thus, letting $k$ denote the edge $e_k = (i \to j)$, we have

$$\Pi_{lk} = \begin{cases} +1, & \text{if } l = j \\ -1, & \text{if } l = i \\ 0, & \text{otherwise.} \end{cases}$$

The polar transport graph is a subgraph of the cell graph and consists only of those cells which are incident to an edge that corresponds to an unknown $\pi_{i\to j}$—there are $n' \leq n$ such cells. In particular, only $n'$ out of the $n$ rows of $\Pi$ have non-zero entries.

**Proposition 2.** *We can compute $\vec{\pi}$—and therefore $\mathbf{p}$—if and only if the polar transport graph is an undirected forest, i.e. $m = n' - c$ ($c$ is the number of connected components), and $\mathbf{c}$ was obtained from a transport rule $\phi$ that satisfies $\phi(i \to j) = -\phi(j \to i)$ for each edge $(i, j)$.*

*Proof.* First, we note that the rank of $\Pi$ is $n' - c$ by Proposition 4.3 in [9, p. 24]. Thus, the non-zero portion of $\Pi$ is square and invertible if and only if $m = n' - c$. Suppose that $\vec{\pi}$ was computed using

this square matrix. The variables satisfy all $n'$ equations, not only the $n' - c$. To see why, note that $\pi_{i\to j}$ appears in exactly two equations but with opposite signs. Also, diffusive transport works in the same way, as did the original transport rule. Thus, both sides of Eq. 11 satisfy the property and $\vec{\pi}$ is a solution to the whole system Eq. 13. □

The exact nature of transport facilitation that PIN1 provides is unknown, but the effective polar transport provides a measure of the effect. Hence, assuming a model of auxin transport by PIN1, we can compute how much protein is needed to achieve the effect through a relation analogous to Eq. 8. In the simplest model the density of PIN1 is only proportional to $\pi$.

# 6 Predictions of Vein Patterns in Leaves

We shall now show that we can not only predict where and when new c-vascular strands form, but also the relative strength of polar transport that implements the required improvement in auxin transport. The the best of our knowledge, PIN1 is a likely and, possibly, paradigmatic instance of molecular polar transport and a precursor to the venation pattern. However, the pattern of PIN1 expression, referred to as PED (or PIN1 expression domain), does not correspond exactly to the vein pattern. Recent experimental studies by Scarpella *et al.* [52] demonstrate that only a subpart of the PED becomes vein pattern. Surprisingly, some parts of the PED disappear. Here, we shall show that our theory is consistent with these observations by showing how each of the major empirically defined stages can be explained within our framework. We shall model the behavior of cells within a developing leaf—the so-called leaf primordium—and the adjoining cells of the shoot apex (see Fig. 3 and Fig. 4). We begin with a cartoon domain of cells, to show qualitative properties, and then proceed to compare these results to experimental data.

## 6.1 Emergence of leaf primordium and formation of midvein

Our model predicts the emergence of a midvein as a result of leaf growth. The formation of a new leaf primordium on the shoot apical meristem (SAM, see Fig. 3) begins by the reorientation of polarity in some cells and the formation of "convergence points"—red arrowheads in Fig. 5. This, as our model predicts, results in the creation of a locally extreme difference in auxin concentration. Fig. 5*B* illustrates that $\Delta c$ is largest near the convergence point between the cell marked with a cross and its neighbor marked with a red star. The large $\Delta c$ promotes PIN1 creation and, eventually, the

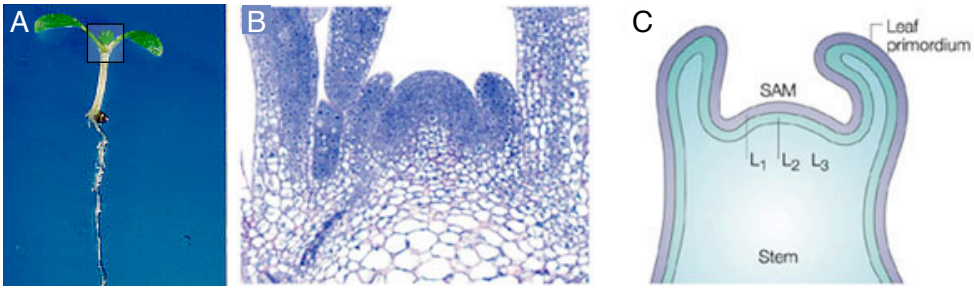


Figure 3: Structure of shoot apex and location of leaf primordium. **(A)** *Arabidopsis thaliana* seedling (from [53]). **(B)** A slice through the shoot apex of *A. thaliana* [31, Fig. 5] found under highlighted area in *A*. **(C)** Schematic of slice in *B*. SAM: shoot apical meristem, responsible for growth along the main axis.

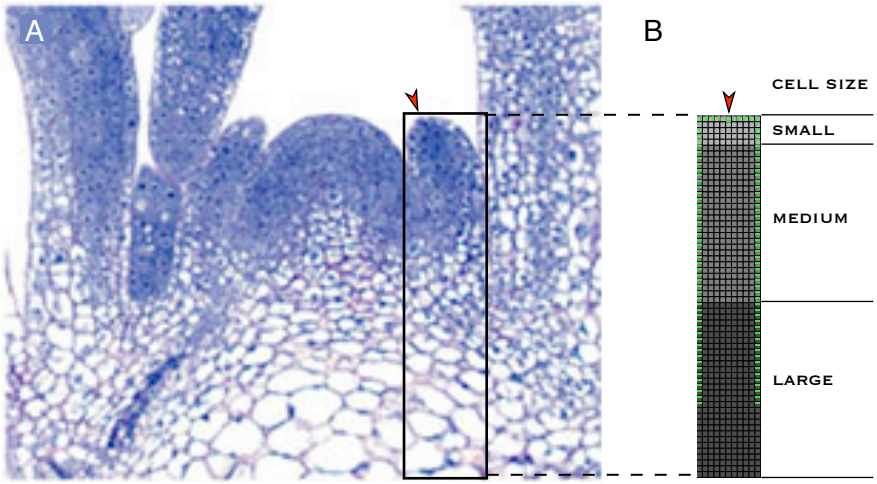


Figure 4: Setup for simulations. **(A)** Shoot apex of *A. thaliana* as in Fig. 3*C*. **(B)** Simulation domain corresponding to region of real organ. Red arrowhead points at tip of leaf primordium. Cell sizes increase moving away from the tip, compare with *A* where cells are largest in the stem.

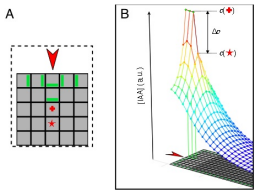


Figure 5: Predictions of auxin concentration during initial stages of primordium formation. **(A)** Magnification of the tip of our simulation domain. Carrier expression localizes asymmetrically and, along the marginal cells, points toward a convergence point—cell with red arrowhead. **(B)** The predicted distribution of auxin. Note that the largest $\Delta c$ is between the cell marked with a red cross and its neighbor marked with a red star. This is the most likely place for new PIN1. As $A$ shows, these cells are at the tip of the inward forming midvein PIN1 expression domain. Exaggerated $c$ for display purposes.

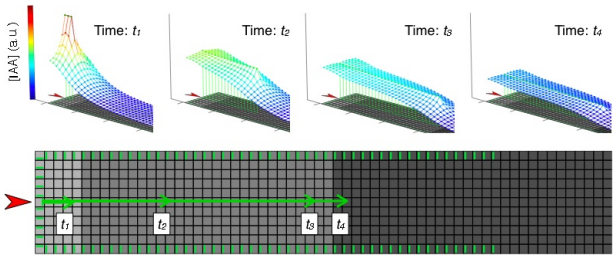


Figure 6: Prediction of midvein from MPED using Algorithm 1. The domain and the marginal PIN1 expression, green bars, are shown. Also shown are four snapshots during the execution of Algorithm 1 labelled $t_1, t_2, t_3$, or $t_4$. The new PED forms where the midvein of the new leaf should be, green arrows. Note that this pattern is not prescribed, but the result of implementing our Schema 1 of [16] as Algorithm 1.

interface on the side of the cell with a cross is endowed with the carrier. Following the extension of the middle PED, the extreme $\Delta c$ moves to the next interface of the cell with the star and the procedure repeats. But each time the PED is extended in this fashion, the extreme $\Delta c$ decreases until it is too small to create any new PIN1 (Section 3).

To illustrate, consider Fig. 6. We are given the marginal PIN1 expression and follow the predictions of our model through time as they give rise to the midvein. At time $t_1$ we show the configuration from Fig. 5. Then new PIN1 appears and creates a large $\Delta c$ at the tip of the PED. Observe that this $\Delta c$ is smaller at time $t_2$ than at time $t_1$. It is even smaller at time $t_3$ and, at time $t_4$, it becomes too small to create new PIN1. So the midvein PED extends a finite distance from the primordium tip toward the stem below.

In fact, these predictions are consistent with experimental observations. Our initial setup mimics the biology, Fig. 7, and our predictions for an extending midvein during leaf growth coincide with

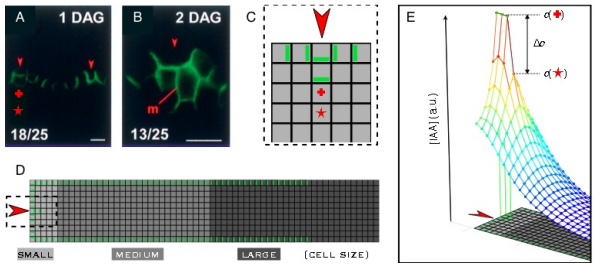


Figure 7: Predictions of auxin concentration during initial stages of primordium formation. **(A,B)** Initial stages in the formation of leaf primordia (from [52]). Sub-cellular localization of PIN1 directed toward so-called "convergence points": cells shown with red arrowheads. **(C)** Model of this behavior. PIN1, depicted in green, organize in marginal PEDs (MPED) facilitating auxin flow toward the tip of the primordium (the convergence point) from all sides. The hormone is evacuated by the inwardly directed PIN1 expression that will eventually become part of the midvein in the new leaf. **(D)** Entire simulation domain. Selected region enlarged in *C*. **(E)** Distribution of auxin concentration at equilibrium computed as described in Section 5. The midvein PED works with diffusion—mode 1—and the MPEDs work against diffusion—mode 2. The largest $\Delta c$ is at the end of the midvein PED between the cell marked with a cross and the neighbor marked with a red star. This is the most likely place for new PIN1. Exaggerated $c$ for display purposes.

the empirical patterns Fig. 8. But our predictions go even further. We compute the relative demand for polar transport along the whole domain under the Constant Gradient Hypothesis. Thus, if the concentration of PIN1 is proportional to this demand we predict the distribution of the carrier throughout the leaf. Fig. 9 provides one example. Note that more auxin carrier is needed in the midvein than in the marginal PEDs, which is consistent with PIN1 expression in a real leaf.

## 6.2 Convergence points on leaf margin

The pattern of PIN1 expression shown in Fig. 9 is maintained as the young leaf grows. In general, when a cell expressing PIN1 divides the daughter cells inherit the polarity of the mother cell. This rule is broken only occasionally, and when that happens a so-called convergence point results. Our model can explain this phenomenon in the following fashion.

First, examine what happens when a cell on the margin divides. Fig. 10 illustrates the distribution of auxin concentration after the new cell membrane (or wall) has formed sufficiently to present a barrier and the concentrations do not change. Notice, in Fig. 10*B*, that the largest difference in concentration is between the two daughter cells and that it suggests that new PIN1 should appear so that the polarity is consistent with neighboring cells. This behavior is generic — Fig. 12*C* demonstrates it for all cells along the margin but it also holds in the midvein.

The situation in the midvein is somewhat different because there are more neighbors and the

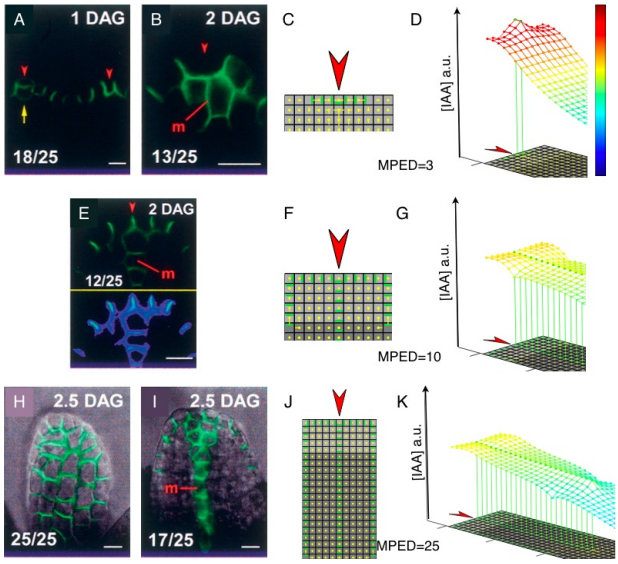


Figure 8: Growth of leaf primordium induces growth of midvein. Note that as the midvein grows, it connects the tip of the leaf—where cells are small so $c$ is high—to cells in the stem—which are large so $c$ is low. Thus, the concentration at the tip of the leaf primordium decreases. In effect, the midvein acts as a straight bar being pushed up at the tip but pulled down near the stem. This is due to PIN1 following Constant Gradient Hypothesis. Three primordium sizes are shown in increasing order: *A–D*, *E–G*, and *H–K*. **(A,B,E,H,I)** from [52].

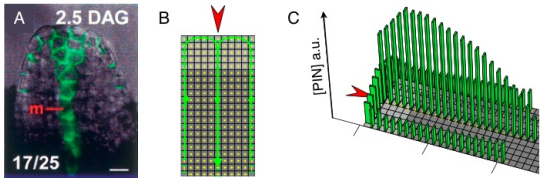


Figure 9: Prediction of PIN1 strength computed as described in Section 5. **(A)** Sample leaf from [52]. PIN1 expression in green, stronger just under tip. **(B)** PIN1 polarity shown as green bars. Flow due to polar transport shown as green arrows. **(C)** Prediction of PIN1 concentration. Height of green bars denotes concentration. The expression is low along the margin and high in the midvein for both the real leaf, in *A*, and predictions, in *C*.

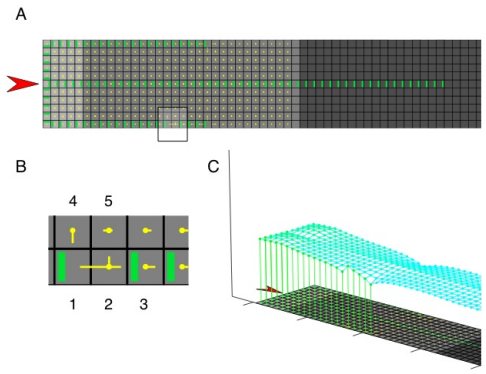


Figure 10: Auxin distribution following a cell division on the leaf margin. **(A)** The domain. Rectangular area blown up in *B*. **(B)** $\Delta c$ shown as a yellow segment starting from the cell with the higher concentration. E.g., the largest $\Delta c = c(2) - c(1)$. Since PIN1 is created due to large differences in concentration and in the direction of that concentration, the new PIN1 accumulates inside cell 2 toward cell 1. Polarity is maintained consistent with neighboring cells. **(C)** Auxin concentration shown as a height map over the domain.

strength of PIN1 is largest in the midvein. Still, Fig. 11 shows that PIN1 polarity can be maintained in the midvein for much the same reasons as before. However, the ensuing difference in concentration through the newly formed interface is significantly larger for a dividing midvein cell than for a dividing margin cell, Fig. 12*D* demonstrates this graphically. As a result, new PIN1 should appear quicker and have an effect on the concentration faster for dividing cells in the midvein than for dividing cells along the margin. Therefore, any PIN1 that may start forming at interfaces other than the new one would probably not form in sufficient quantity to remain there after the new interface has acquired its share of PIN1.[4] The cells along the leaf margin, on the other hand, cannot create $\Delta c$ quite as large and the ensuing slower acquisition of PIN1 can result in PIN1 appearing—and persisting—at interfaces other than the newly created one.

The most interesting phenomenon of this sort is the flip of polarity at a nearby interface, which creates a convergence point: a stable discontinuity of PIN1 polarity along the margin. Fig. 12*B* illustrates the differences in concentration resulting from a cell division that created cells 2 and 3. Besides the largest $\Delta c$ through the new interface, there are other interfaces with non-trivial $\Delta c$. Fig. 12*C* plots three of the largest $\Delta c$ as a function of the location of the dividing cell along the margin. Of the three, only the $\Delta c$ through interface $1 \rightarrow 2$ can break the continuity of polar cells and create a "flip". The most likely location for such a flip is where $\Delta c$ is largest and it is possible

[4] In other words, the fast action of PIN at new interface will not allow the $\Delta c$ at neighboring interfaces to exceed $\tau_1$ long enough to make $p > p_\tau$ at the neighboring interfaces. Here $\tau_1$ is such that the PIN1 dynamics can, given sufficient time, switch to the "on" position, i.e. $[PIN1] > p_\tau$.

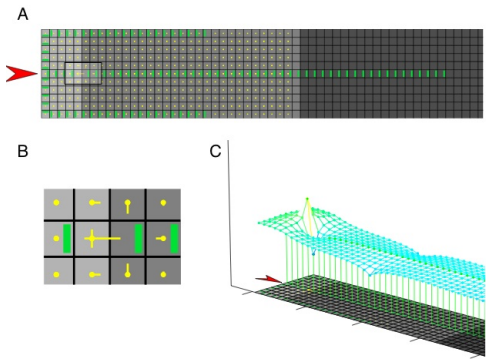


Figure 11: Auxin distribution following a cell division at the midvein PED. **(A)** The domain. Rectangular area blown up in *B*. **(B,C)** Largest $\Delta c$ through new interface as in Fig. 10.

for a flip to remain there. Fig. 13 illustrates a likely sequence of events that results in a stable flip of polarity. In particular, this gives rise to the so-called convergence point on the margin. The stability of this discontinuity is due the relatively slower dynamics of PIN1 along the margin as compared to the midvein are important here. If a flip were to occur in the midvein, then the resulting $\Delta c$ against the action of PIN1 will grow faster than the neighboring interfaces can compensate and, eventually, will make PIN1 flip back. Hence, the flip will be unstable in the midvein.

## 6.3 Formation of the first loop

Once a convergence point has been established the pattern of PIN may continue progressing inwardly in a manner similar to the midvein appearance (Section 6.1). On the other hand, the convergence point may remain stable for a while—i.e. observable in experiments—and, we predict, the strand connecting it to the midvein may emerge according to slightly different dynamics. Fig. 14*A* shows that the largest $\Delta c$ is near the midvein while the peak of concentration is at the convergence point. Accordingly, the new strand will emerge at the midvein first and make its way to the convergence point—just like a new strand in an areole progresses from the existing vein toward the peak of concentration (e.g., see [16]).

In fact, dynamics much like the ones discussed for areoles predict the next step in the elaboration of the first loop. The PIN expression domain in Fig. 14*B* that includes the portion of the margin between the tip and the convergence point, the midvein and the newly created strand form, geometrically, an areole. Surprisingly, the distribution of auxin concentration in this geometric areole looks very much like the distributions from [16] and [14] as Fig. 14*C,D* illustrate: low concentration along

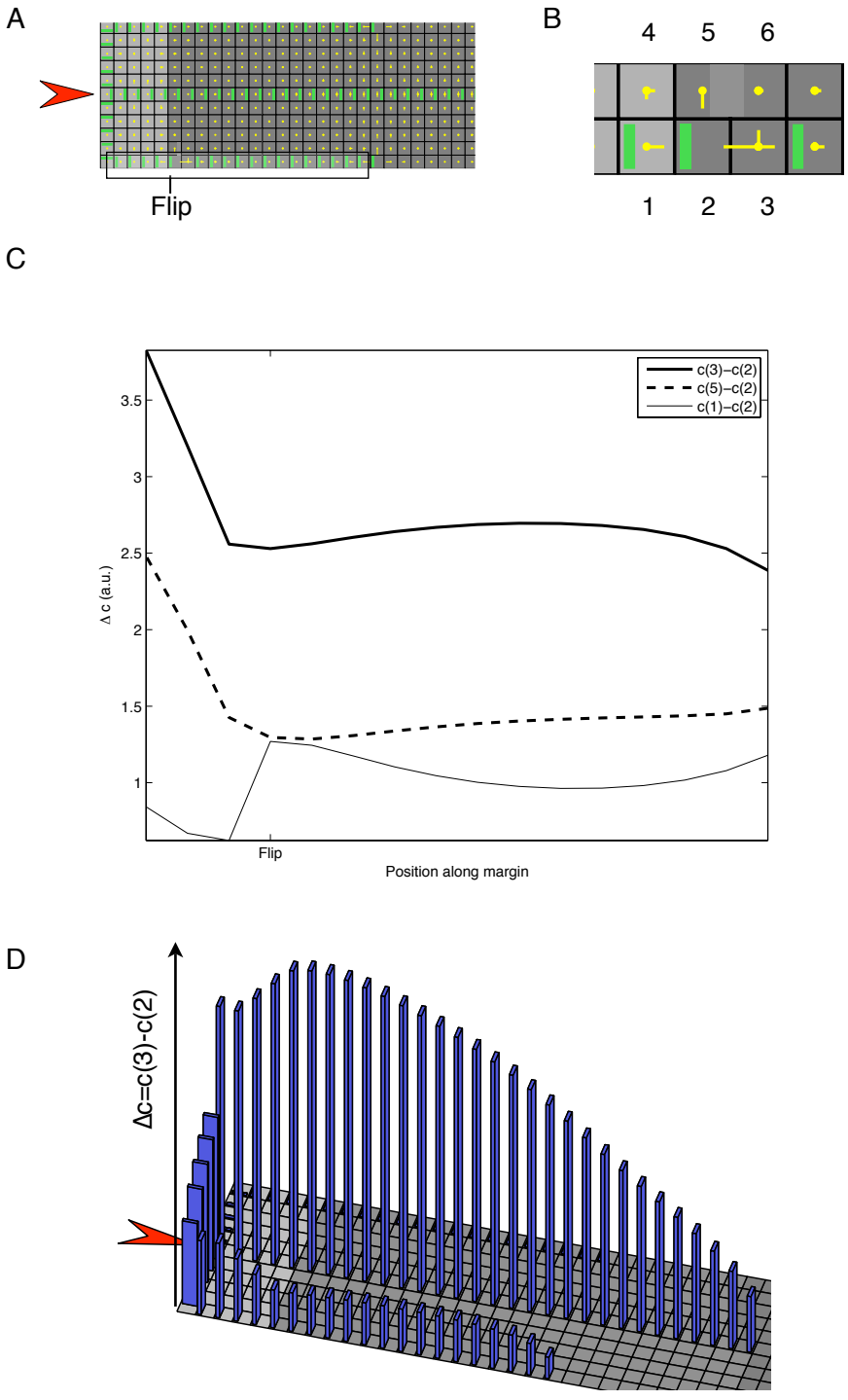


Figure 12: Cell division effects along leaf margin. **(A)** The rectangle encloses the cells used in $C$. Example of one cell dividing while all others do not. **(B)** The neighborhood of a cell that has recently divided. The daughter cells are labeled by the numbers 2 and 3, and the new interface between them does not yet express PIN. The curves in $C$ are obtained by sliding this neighborhood along the margin (rectangle in $A$): think of the position of cell 1 as moving along the margin, while the other compartments have positions relative to that of cell 1. **(C)** Three curves obtained from measuring $\Delta c$ as indicated. **(D)** Effect of cell division along the whole PED. Hormone distribution computed for each location separately assuming that a cell has divided at that location only (as in Fig. 10 or Fig. 11). Height of bar is $\Delta c$ through the new interface without PIN. Aggregate plot.

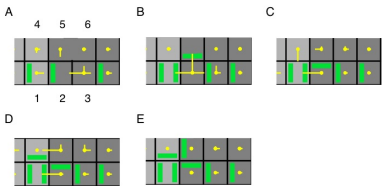


Figure 13: Creation of a convergence point at the leaf margin due to a cell division. PIN1 is created where $\Delta c$ is large in the direction of arrows; destroyed if against such arrows. **(A)** Initial configuration. Cell divided into cells 3 and 2. Expect new interface to acquire PIN1 $3 \to 2$. However, $\Delta c$ at $1 \to 2$ is large enough, so PIN1 will flip there. Also, $5 \to 2$ will be created. **(B)** The predicted configuration form *A*. The largest $\Delta c$ is against the PIN1 acting $5 \to 2$ so polarity will flip. **(C)** Updated configuration from *B*. **(C,D)** If the supporting PIN1 can appear fast enough, then the $\Delta c$ through $2 \to 1$ will not eliminate the original flip and the configuration will be stable as in *E*. **(E)** Stable configuration: there are no more high $\Delta c$. Cell 1 is a bipolar cell because PIN expresses on both its left and right interfaces. Cell 2 is a convergence point because cells on both sides exhibit polar transport toward cell 2.

boundary, peak inside, and highest $\Delta c$ at the boundary. The new strands inside this geometric areole can be predicted by following the largest $\Delta c$ as discussed in [16] and the companion paper [14]—we obtain Fig. 15.

The key difference, however, is that the boundary PED of the areole is not entirely stable. The interface of the bipolar cell with the convergence point actually expresses PIN in the direction against diffusion. Thus, a sufficiently quick infusion of auxin into the convergence point cell can increase $\Delta c$ enough to cause a flip, remove the bipolar cell, and reestablish the continuity of PIN1 polarity along the margin. Such an infusion can result from the creation of the new strand.

Indeed, as Fig. 15 illustrates, the extension of the PED in the geometric areole can remove PIN from some interfaces. As the new PIN expression emerges (Fig. 15*A*), the right hand side strand is infused with additional auxin. Even though the strand may potentially adapt to the new demands—by increasing the amounts of PIN that drain the hormone away—any adaptation requires time during which the whole strand will see higher overall concentrations. This is especially important at the convergence point where, in particular, the $\Delta c$ through the interface with the bipolar cell (red bar in Fig. 15) will rise. Since, as we argued in [14], the new strand (solid arrow) is likely to extend in quick bursts, the infusion of auxin into the CP is likely to increase this $\Delta c$ and flip the PIN expression. Once that happens, the PED connecting the margin to the midvein will gradually disappear as well—the stability of the convergence point requires all of the supporting structure as illustrated in Fig. 13.

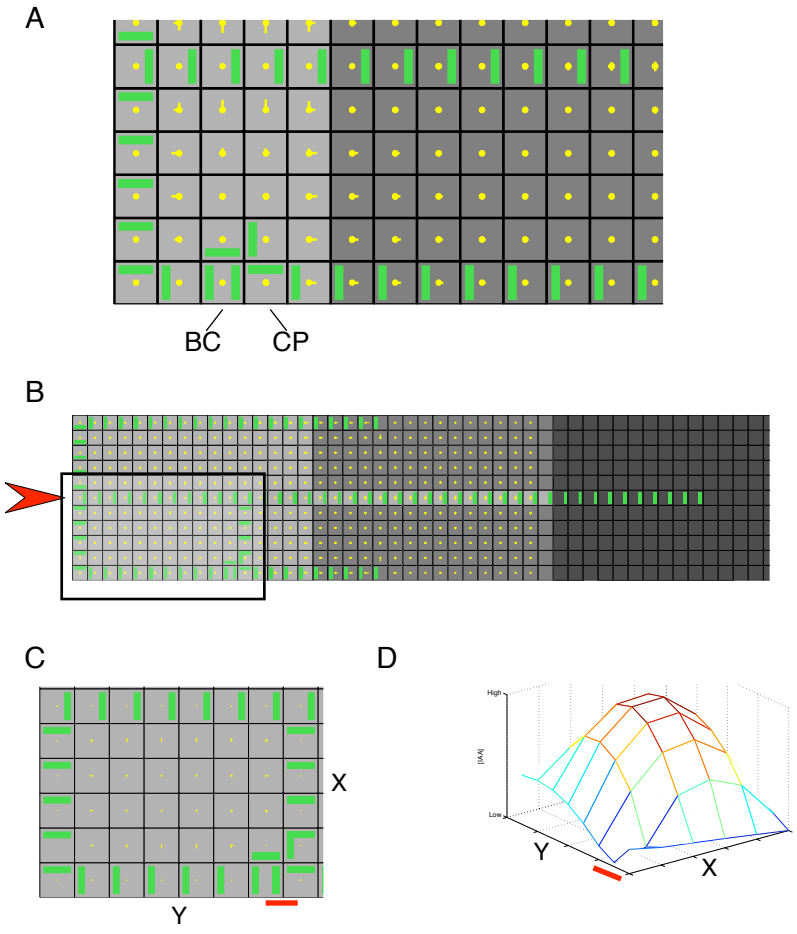


Figure 14: Emergence of strand connecting convergence point (CP) to midvein; creation of geometric areole. **(A)** Distribution of $\Delta c$. Notice that the $\Delta c$ at the convergence point is zero so there is a peak of concentration there. Conversely, the largest $\Delta c$ is at the midvein, so a new strand could emerge from the midvein and end at the convergence point by following the usual local rules. BC: bipolar cell; CP: convergence point. **(B)** Domain with new strand. Rectangle encloses the geometric areole. **(C)** Close up of geometric areole. Note the red bar under the interface between the BC and the CP. **(D)** Concentration, $c$, of auxin in geometric areole. Red bar corresponds to red bar in $C$. Note that $c(CP) > c(BC)$ so PIN1 works against diffusion and an auxin infusion into CP can flip the polarity of the interface between BC and CP.

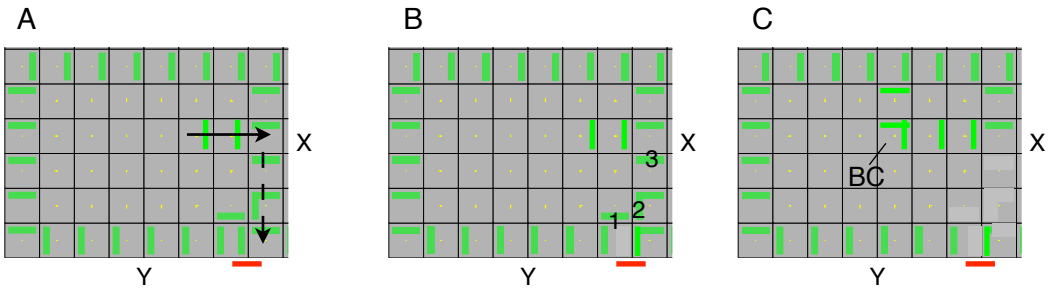


Figure 15: Formation of first loop. **(A)** The new PIN expression as predicted by our model is shown (solid arrow). This increases auxin supply into the strand along $X$, which causes the concentration to increase there. Since the midvein cannot drain the new infusion of auxin immediately—adaptation time—there is a back propagation effect (dashed arrow) which causes the concentration of auxin to increase even at the convergence point (CP). **(B)** The bipolar cell disappears since the PIN between BC and CP flips sides due to the increased $\Delta c$ caused by the new strand. As this happens, the PIN at interface 1 starts pushing auxin against the gradient and eventually disappears. Next, interfaces 2 and 3 disappear for the same reason. **(C)** The new strand meets in the middle of the areole—where the concentration peak is—creating a bipolar cell there (BC) but the connection to the margin is now lost.

# 7 PIN Patterning in the *Arabidopsis* Embryo

The same Non-linear Polar Transport model which accounts for many key events during vein formation also explains key patterning events at the earliest stages of plant development: the embryo formation. Fig. 16 shows how to obtain the geometry of embryos from images of the tissues. Then, in Fig. 17 and Fig. 18 we show how the polar pattern of PIN expression is predicted by our model.

We begin with the assumption that no polar pattern exists. Uniform expression of PIN is equivalent to diffusion transport—as we argue in Appendix Section A—so our Helmholtz model suffices to predict the initial distribution of auxin concentration for an embryo in the globular stage, Fig. 17*A,B*. This distribution exhibits a maximal difference in concentration between the suspensor cells numbered 24 and 25 which, according to Schema 1, makes that interface the most likely first location for strong PIN expression. As this happens, the $\Delta c$ there decreases and causes PIN to appear in several other suspensor interfaces, as shown in Fig. 17*C*. In turn, this event causes the $\Delta c$ between the suspensor cell 24 and its neighboring embryo cells to increase significantly, and polarizes the expression of PIN at those interfaces. This polarization continues into the embryo—like the formation of a new strand in an areole—until it reaches the smallest cells: cell 5 and cell 6 in Fig. 18*A*. At that point no significant $\Delta c$ exists in the globular stage embryo. The triangular stage, resulting from several cell divisions, presents a different cell size distribution and significant

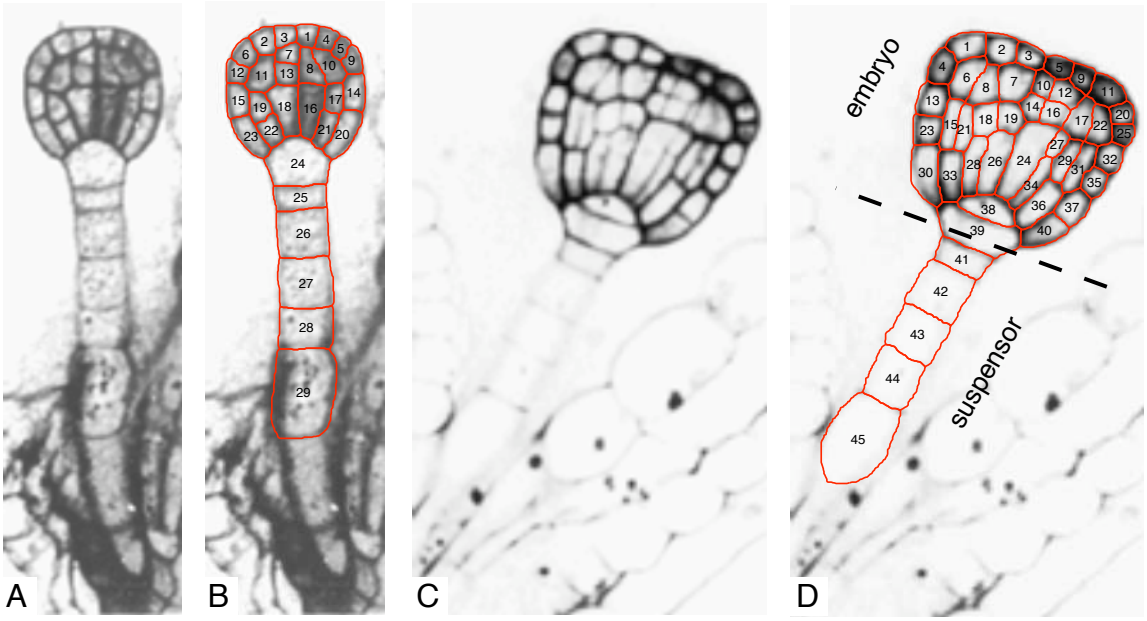


Figure 16: Obtaining the geometry of *Arabidopsis* embryos. **(A)** Globular stage (from [11]). **(B)** Domain extraction from *A* following the procedure in Section C. Embryo: cells 1 through 23; suspensor: cells 24 through 29. **(C)** Triangular stage (from [11]).

$\Delta c$ appear again, Fig. 18*B*. In fact, a convergence point appears near cell 11 due to the established pattern of PIN from the earlier stages.

The final predicted pattern, shown in Fig. 18*C* and Fig. 19*C*, captures two important qualitative characteristics observed in the lab: one regarding the emergence of new leaves and one regarding the root tip. The theory developed here explains the initial formation of the 'convergence point' patterns that mark the appearance of new leaf primordia. In the case of the embryo, these are the cotyledons, but the same process could be taking place near the shoot meristem in mature plants. The theory also explains why the polarity of PIN in the root is towards the root tip. That is the result of the original differences of cell size. The suspensor cells, being larger, produce auxin at a lower per-volume rate than the embryo cells, so suspensor cells are predicted to have a lower concentration of auxin. Thus, the difference in concentration sets up the polar pattern near the root tip, which will be maintained through development due to the memory-like behavior of PIN dynamics. In a companion paper [15] we shall show that this initial pattern sets the stage for the observed 'reflux' pattern in mature roots, and that the Polar Transport model developed here explains the events that lead to the mature pattern as well.

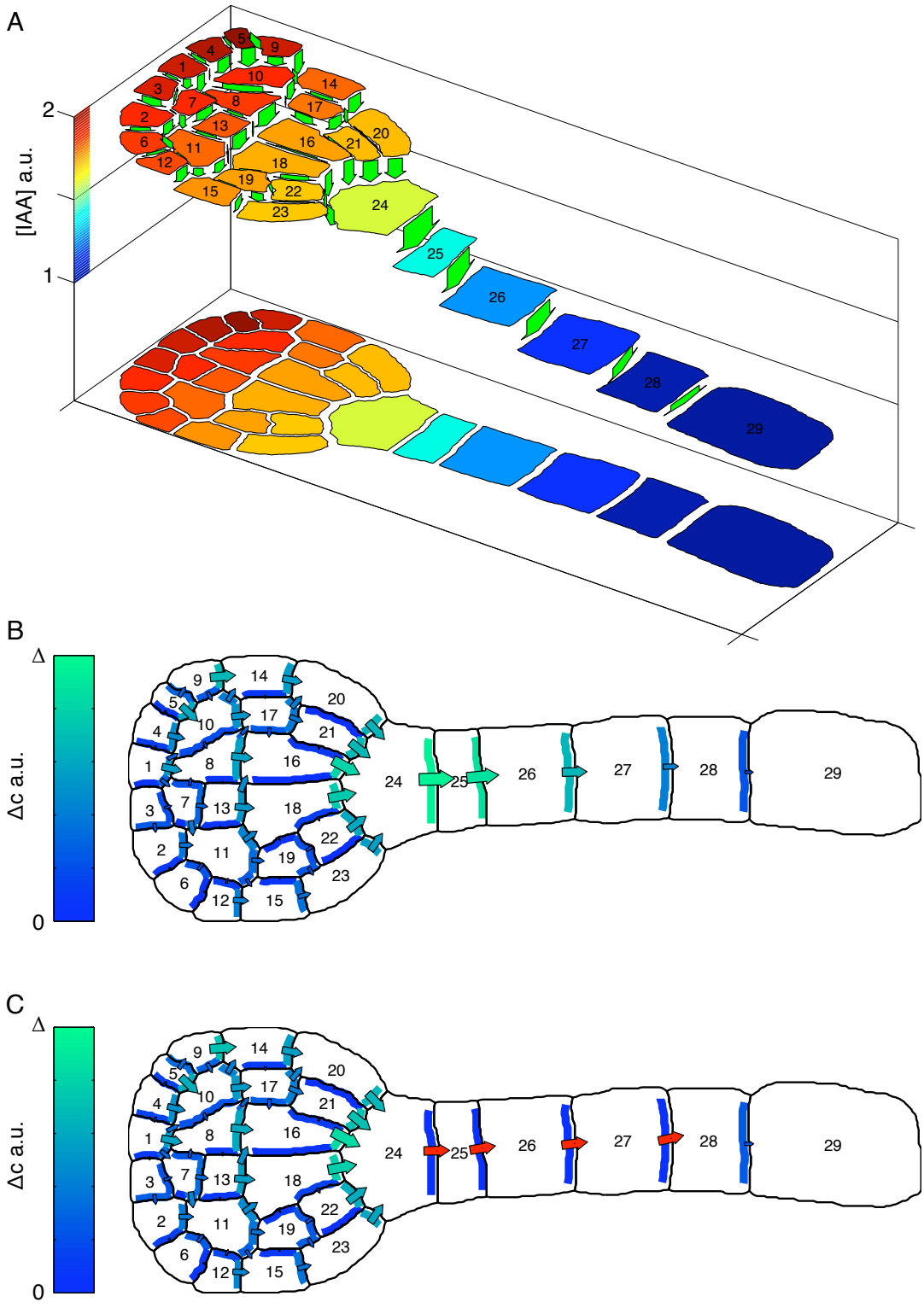


Figure 17: Prediction of PIN pattern in embryos. **(A)** Concentration of auxin assuming Helmholtz conditions, i.e. no polar transport. **(B)** Differences of concentration, $\Delta c$, for auxin distribution as in $A$. Arrow size proportional to $\Delta c$. Note largest $\Delta c$ between suspensor cells 24 and 25: PIN should appear there first. **(C)** $\Delta c$ after introducing some of predicted polar transport (red arrows). Note large $\Delta c$ between suspensor cell 24 and the embryo: PIN should form there next.

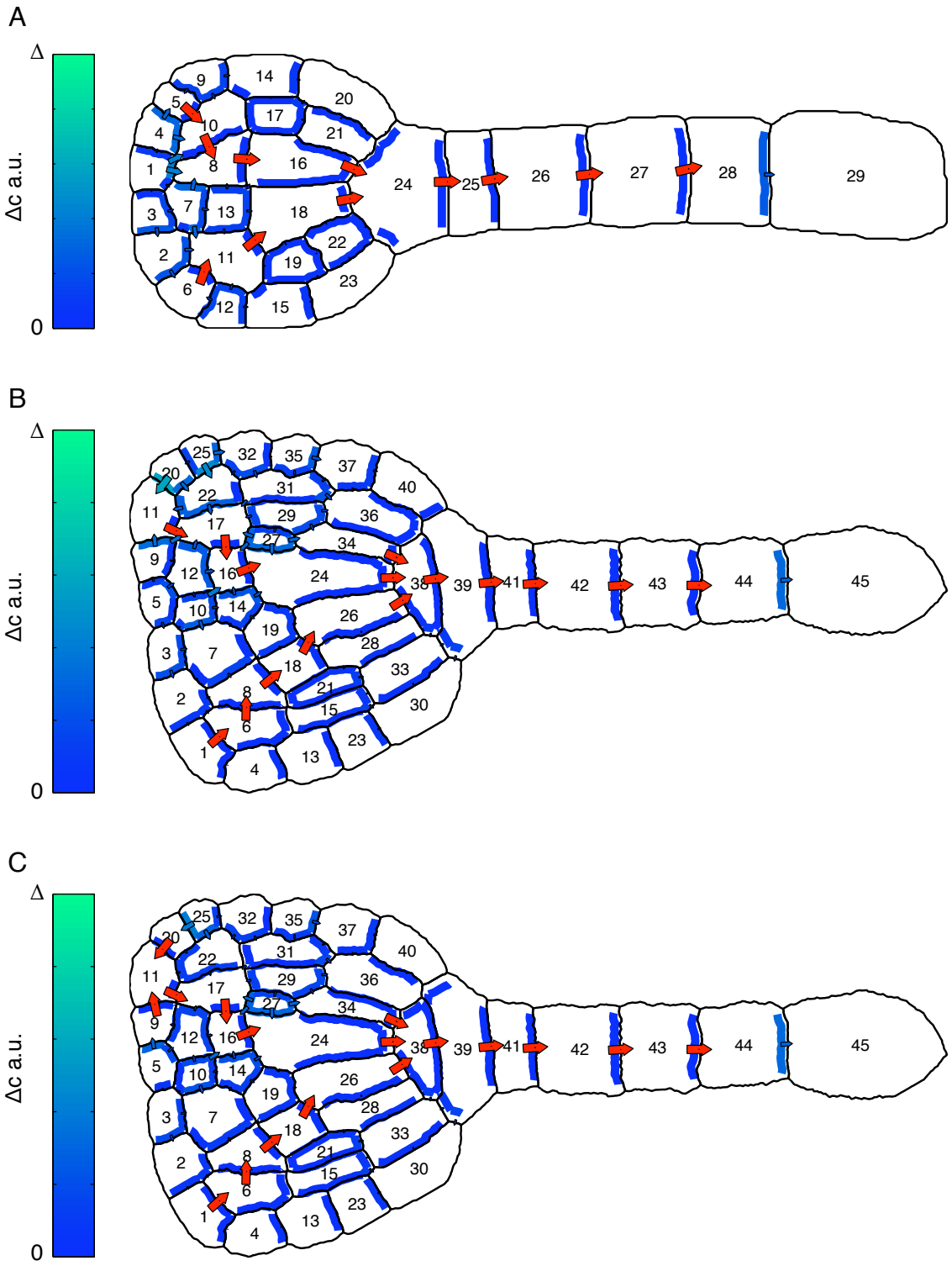


Figure 18: Prediction of PIN pattern formation in embryos (continued). **(A)** Predicted PIN pattern by following $\Delta c$. No more large $\Delta c$ exist. **(B)** $\Delta c$ in a triangular stage embryo with established PIN pattern. Note that the new cells (size distributions) create a non-trivial $\Delta c$ between cells 20 and 11: PIN should form there next. **(C)** Final PIN pattern predicted by our model. Note the 'convergence point' at cell 11. Blue (color coded) arrows show $\Delta c$—size represents value. Red arrows represent polar transport—their size does not indicate strength.

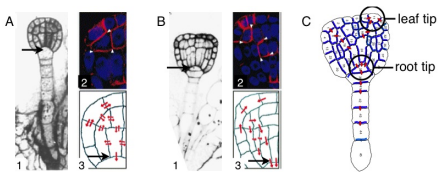


Figure 19: Prediction of polar expression of PIN in *Arabidopsis* embryos and comparison to real measurements. **(A)** Globular stage. **(B)** Triangular stage. Note that the suspensor cells are larger than the embryo cells. Hence, our Helmholtz model predicts higher concentration in the embryo than in the suspensor. Black arrows point at where the root tip will be. Insets 1 from [11]; insets 2 and 3 from [5]. **(C)** Our model predicts the typical polar transport patterns in both the leaf primordium and near the root tip: (1) the 'convergence point' pattern near the embryo tip where a leaf primordium will emerge (a cotyledon); and (2) the polarity of PIN expression is toward the root tip and due to the larger suspensor cells.

# 8 Conclusion

The diversity of phenomenology, data, and temporal information about plant development is difficult to unify unless an abstract perspective is taken. In this series of two papers we sought to articulate several of the basic principles that could underlie the developmental biology of plants, and to place these within a mathematical framework that allowed their consequences and implications to be calculated.

Realizing that distance information is fundamental, we introduced three principles that could work together within a reaction-diffusion model to predict how global distance information could be signalled locally, at the cell level. The first two principles, that auxin is produced at a constant rate in each cell and is destroyed in proportion to concentration, yielded models that predicted qualitative auxin distributions. Together with a simple schematic rule that cells begin to convert from a ground to a vascular state provided the concentration difference exceeds a limiting value led to a model of vascular formation.

In this paper we elaborated this schema to a more realistic biophysical level. Facilitated transport of auxin by carriers such as those in the PIN and AUX families serves to effect the ground-to-vascular transition, but it does so in the context of non-linear dynamics with substantial predictive power. While it is widely accepted that PIN patterns prefigure vascular patterns, we were able to show that this dynamic— including the discrete and specialized structures that arise within it during plant development—can be predicted. Simulations showed how the leaf primordium emerges, how convergence points arise on the leaf margin, how the first loop is formed, how the intricate pattern of PIN shifts during the early establishment of vein patterns in incipient leaves of Ara-

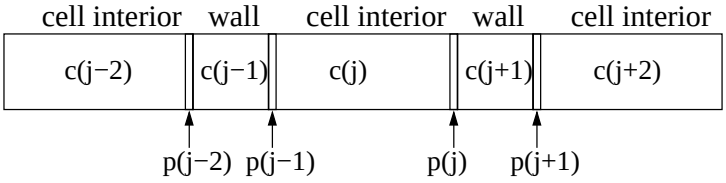


Figure 20: Schematic depiction of cells (compare with [26, Fig. 1]). Five major compartments are shown: three cell interiors and two cell walls. The permeabilities through the plasmalemma are shown for all four compartment junctions and denoted by $p(i)$.

bidopsis, and how the midvein forms. Most importantly, we showed how the embrio provides an initial configuration sufficient to get it all started.

Just as principles provide the foundation for theoretical physics, and mathematics provides the machinery to realize their consequences, we have sought to provide an abstract view of the development of pattern structure in plants. Our principles were designed to articulate key aspects of plant biology when viewed from an abstract, "high in the air" perspective. We believe they will hold as the facts relating to auxin production, destruction, and facilitated transport develop further; and that their predictions will lead to further experiments revealing the beauty and subtlety of plant development.

# A Simplification of the Chemiosmotic Model

We now show that the net effect of active transport as predicted by the chemiosmotic theory may be captured by a small extension to our earlier model. Specifically, we show that the same effect may be obtained without the need to introduce separate compartments for cell interiors and cell walls—it suffices to keep the interior of cells as discrete compartments and to introduce the effect of carriers as directional active transport coefficients. These coefficients are a direct measure of the net effect of facilitated auxin transport, which we develop in the main body of the paper.

Suppose, then, that we have a system of five compartments as in Fig. 20. Let $J(j \to j+1)$ denote the mass flux between compartments $j$ and $j+1$, so $J(j \to j+1) = -J(j+1 \to j)$. Define $\Phi(j \to j+2)$ as

$$\Phi(j \to j+2) = \frac{J(j \to j+1) + J(j+1 \to j+2)}{2}. \tag{14}$$

Our task is to show that it is possible to think of $\Phi(j \to j+2)$ only in terms of the compartments $j$ and $j+2$, the cell interiors.

We do this by examining the behavior of the system at equilibrium. The substance is only produced inside cells and it is also depleted there by various metabolic processes. The following equations formalize these assumptions:

$$\begin{array}{lll} (1) & J(j-2\to j-1)+J(j\to j-1) & = 0 \\ (2) & J(j-1\to j)+J(j+1\to j)+\rho(j)-\alpha c(j) & = 0 \\ (3) & J(j\to j+1)+J(j+2\to j+1) & = 0 \\ (4) & J(j-1\to j-2)+\rho(j-2)-\alpha c(j-2) & = 0 \\ (5) & J(j+1\to j+2)+\rho(j+2)-\alpha c(j+2) & = 0 \end{array} \tag{15}$$

The concentration of the substance in each compartment is assumed to be uniform and is denoted by, e.g., $c(j)$ for the middle cell interior. Each equation corresponds to a compartment. The first three describe the cell wall $c(j-1)$, the middle cell interior $c(j)$, and the second cell wall $c(j+1)$. The last two equations describe the equilibrium dynamics of the leftmost and rightmost cell interiors, respectively. The production of the substance is captured by $\rho$ and the destruction by $\alpha c$ with $\alpha$ a constant. Let $T(j)=\rho(j)-\alpha c(j)$ and write the dynamics (at equilibrium) of the cell interiors assuming that the cell membranes and cell walls together are a single interface and that $\Phi$ describes the flux through those interfaces:

$$\begin{array}{lllll} (a) & \Phi(j-2\to j)+\Phi(j+2\to j)+ & T(j) & = & 0 \\ (b) & \Phi(j\to j+2)+ & T(j+2) & = & 0 \\ (c) & \Phi(j\to j-2)+ & T(j-2) & = & 0 \end{array} \tag{16}$$

It is easy to check that Eq. 16 can be obtained from Eq. 15 by the following linear combinations:

$$\begin{array}{lll} (a) & := & \frac{(1)+(2)+(2)+(3)}{2} \\ (b) & := & \frac{(3)+(5)+(5)}{2} \\ (c) & := & \frac{(1)+(4)+(4)}{2} \end{array}$$

Thus, if the $\Phi$ flows only depend on the concentrations in three of the five compartments, then Eq. 16 has a unique solution which is compatible with the chemiosmotic theory. We now derive the conditions under which this holds and, therefore, demonstrate that our simulations are in agreement with the chemiosmotic theory.

The substance is a weak acid and that the concentration $c=[HA]+[A^-]$, i.e. the total

concentration of protonated (associated) acid and the concentration in ionic form (dissociated). The dynamics of $c$ depend on the dynamics of both $[HA]$ and $[A^-]$, so we need to express each one as a function of $c$. Noting that the dissociation of a weak acid is given by the reaction

$$HA \rightleftharpoons H^+ + A^-; \quad K_a = \frac{[H^+][A^-]}{[HA]} \text{ mol} \cdot \text{l}^{-1}$$

we write

$$K = \frac{[H^+][A^-]}{[HA]} \Longrightarrow [HA] = \frac{10^{-pH}[A^-]}{10^{-pK}} \Longrightarrow [A^-] = [HA]10^{pH-pK}$$

which together with $c = [HA] + [A^-]$ gives

$$[HA] = \frac{1}{10^{pH-pK}+1}c \quad \text{and} \quad [A^-] = \frac{10^{pH-pK}}{10^{pH-pK}+1}c \quad . \tag{17}$$

The change of total concentration due to substance transport is the result of two simultaneous effects: (1) the protonated form $HA$ diffuses through the membrane, and (2) the anion $A^-$ moves across the membrane as a result of auxin carriers and the electrical potential established by the difference in $pH$ between the interior and exterior (cell wall) of the cell [26]. This dynamical behavior is therefore (see, e.g., [27]):

$$J(i \to e) = P_{HA}\left([HA]_e - [HA]_i\right) + P_{A^-}g(V)\left([A^-]_e - [A^-]_i f(V)\right) \tag{18}$$

where $P_{HA}$ is the permeability of the protonated acid; $P_{A^-}$ is related to the amount of auxin carriers on the membrane; $V$ is the membrane voltage; the subscript $e = j+1$ and $i = j$ denote the exterior and the interior of a cell, resp.; $f(V) = \exp(\phi)$ for $\phi = -FV/RT$, an electrical term consisting of the Faraday constant $F$, the gas constant $R$, and absolute temperature $T$; $g(V) = \frac{\phi}{1-f(V)}$. We do not include the diffusion of $A^-$ through the membrane because it appears to be negligible [4, 28, 29].

Let $\beta_j = 1/(10^{pH_j-pK}+1)$ and $\alpha_j = 1-\beta_j$. Let $h = g(V)f(V)$ and, using Eq. 17, rewrite Eq. 18 as

$$J(j \to j+1) = P_{HA}\left(\beta_j c(j) - \beta_{j+1}c(j+1)\right) + P_A(j)g\left(\alpha_j c(j) - f\alpha_{j+1}c(j+1)\right)$$

It is reasonable to assume that $f_j = f_{j+2}$ because both functions relate the interior to the exterior of the cell in the same order and the voltage appears to be the same. However, the voltage

has opposite sign when the order is reversed, so that $f_j = -f_{j+1} = 1/f_{j+1}$. Therefore, setting $f = f_j$, we obtain

$$J(j{+}1 \to j{+}2) = P_{HA}\left(\beta_{j+1}c(j+1) - \beta_{j+2}c(j+2)\right) + P_A(j{+}1)fg\left(\alpha_{j+1}c(j+1) - \frac{1}{f}\alpha_{j+2}c(j+2)\right)$$

We can now write $2\Phi(j \to j+2) = J(j \to j+1) + J(j+1 \to j+2)$ as

$$\begin{aligned} 2\Phi(j \to j+2) = P_{HA}\left(\beta_j c(j) - \beta_{j+2}c(j+2)\right) \quad &+ \quad P_A(j)g\alpha_j c(j) + \left(P_A(j+1) - P_A(j)\right)fg\alpha_{j+1}c(j+1) \\ &- \quad P_A(j+1)g\alpha_{j+2}c(j+2) \end{aligned} \tag{19}$$

Substituting $P_A(j) = P_A + p(j)$ we can rewrite Eq. 19 as

$$\begin{aligned} 2\Phi(j \to j+2) = \quad & P_{HA}\left(\beta_j c(j) - \beta_{j+2}c(j+2)\right) + P_A g\left(\alpha_j c(j) - \alpha_{j+2}c(j+2)\right) \\ + \quad & p(j)g\alpha_j c(j) - p(j+1)g\alpha_{j+2}c(j+2) + \left(p(j+1) - p(j)\right)fg\alpha_{j+1}c(j+1) \end{aligned} \tag{20}$$

Now if $p(j+1) = p(j)$—in case both sides of the cell have the same permeabilities—then the last term becomes zero. In fact, even if the permeabilities are different the term can be ignored because $fg \sim \frac{1}{100}$ according to the best available estimates (i.e. $V = -120\text{mV}$). Also, since the $pH$ difference between the inside and the outside of a cell is assumed to be the same for all cells (metabolically maintained), we can write $\beta_j = \beta_{j+2} = \beta$ and $\alpha = 1 - \beta$. Eq. 20 becomes

$$2\Phi(j \to j{+}2) \sim P_{HA}(1-\beta)(c(j) - c(j{+}2)) + P_A g\beta(c(j) - c(j{+}2)) + g\beta(p(j)c(j) - p(j{+}1)c(j{+}2))$$

so assuming w.l.o.g. that $p(j+1) = 0$ (i.e. because $P_A = P(j+1)$) and collecting terms

$$2\Phi(j \to j+2) \sim \left(c(j) - c(j+2)\right)\underbrace{\left(P_{HA}(1-\beta) + P_A g\beta\right)}_{\text{Diffusion coeff.}} + \underbrace{g\beta p(j)c(j)}_{\text{Polar transport}} \tag{21}$$

Hence, the flux of auxin between cells can be written as the flux between cell interiors as

$$2\Phi(j \to j+2) \sim D(c(j) - c(j+2)) + P(j)c(j) \tag{22}$$

Note that if the auxin carriers are homogeneously distributed on the cell membrane or if there are none, then $P(i) = 0$ and the flux is governed by Fick's Law. If, however, the carriers are only

located on one side of the cell, then $P_A = 0$ and $P(i)$ in Eq. 22 describes the effect completely. In particular, $P(i)$ is proportional to the amount of carriers on the portion of membrane of cell $j$ adjacent to cell $j + 2$ (as in Fig. 20).

# B Midvein PED prediction

Here is the algorithm used in Section 6.1. It is possible to predict the length of the midvein by measuring the length (or size) of the marginal PIN1 expression, the MPEDs. We fix a threshold $\tau_1$ on $\Delta c$ for the formation of new PIN1 and measure the MPEDs. We obtain $c$ as in Section 5 by first assuming that PIN1 works against diffusion in MPEDs—mode 1—and with diffusion in the midvein PED (if such a PED exists)—mode 2. We check each interface where PIN1 exists against the computed $c$ and change its operation mode accordingly. If all interfaces are consistent with $c$, then we find the largest $\Delta c$ in the domain and check whether it is above $\tau_1$. We extend the PED if $\Delta c > \tau_1$; otherwise, we finish the procedure. This procedure is collected in Algorithm 1 and illustrated in Fig. 6. We can predict the new PEDs in this way provided that the marginal expression of PIN1 is known.

# C Geometric Domain Definition using Voronoi Diagrams

Assuming that auxin diffuses much faster inside the cell than through the cell wall, we do not need to model auxin transport inside the cell, only between neighboring cells. This is the basis of the simulations in Ref. [14], for example, but the geometry and topology of real cells is not accurately captured there. In particular, the neighbor relations are inaccurate as are the sizes of the interfaces. Our approach based on Voronoi diagrams solves this problem. We now describe how arbitrary geometric domains with the required properties can be defined from the Voronoi diagram of a collection of points, and then demonstrate how images of plant tissues can be segmented into cells using this approach. The pseudo-code for the procedure is presented in Algorithm 2.[5]

Consider Fig. 21*A,B*. Two dimensional points (open circles) are defined and the Voronoi diagram computed. The diagram consists of straight line segments that join the so-called Voronoi vertices (represented by asterisks). Each segment is closest to two exactly points and runs through part of the line that divides the plane at halfway between the two points. Some points are surrounded by

[5]The algorithms as presented here are fairly inefficient—they run in $O(n^2)$ time and space. In practice, $O(n \log n)$ times were achieved with appropriate data structures.

**Algorithm 1** Prediction of midvein from MPEDs. $Mode(i, j)$ denotes the action of PIN1 from cell $i$ to cell $j$ and can be: 0 for no action, 1 if against gradient, and 2 if with gradient.

INPUT: Domain with MPED, $\tau_1$
OUTPUT: Domain with MPED and midvein PED
midveininincreased := true
**while** midveininincreased == true **do**
    midveininincreased := false
    consistent := false
    **while** consistent == false **do**
        consistent := true
        Compute $c$ as in Section 5
        **for all** Neighbors $i$ and $j$ **do**
            **if** $c(i) > c(j)$ and $Mode(i, j) \neq 0$ and $Mode(i, j) \neq 1$ **then**
                $Mode(i, j) = 1$, consistent:=false
            **end if**
            **if** $c(i) < c(j)$ and $Mode(i, j) \neq 0$ and $Mode(i, j) \neq 2$ **then**
                $Mode(i, j) = 2$, consistent:=false
            **end if**
        **end for**
    **end while**
    Find $i, j$ neighbors and $\Delta c = c(i) - c(j)$ where $|\Delta c|$ is largest
    **if** $\Delta c \geq \tau_1$ **then**
        $Mode(i, j) = 1$, midveininincreased=**true**
    **end if**
    **if** $\Delta c \leq \tau_1$ **then**
        $Mode(j, i) = 1$, midveininincreased=**true**
    **end if**
**end while**

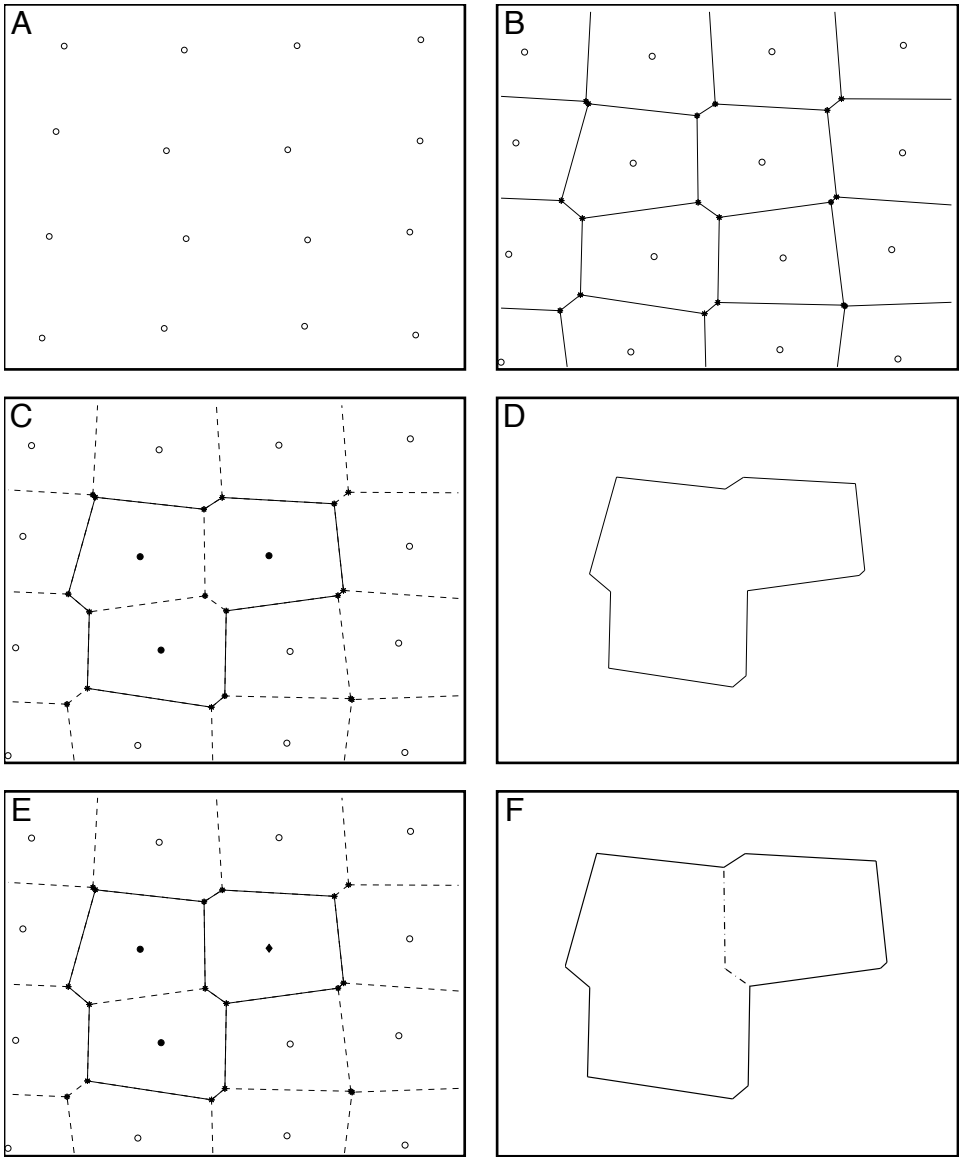


Figure 21: How to use Voronoi diagrams to draw. **(A)** Points in 2-D. **(B)** Voronoi diagram of points in *A*. Voronoi vertices (asterisks) are joined by Voronoi edges or segments (lines). **(C)** Two groups of points: open circles and closed circles. Boundary between two groups (solid line) represents shape in *D*. **(D)** Shape from *C*. **(E)** Three groups of points. **(F)** Shape now consists of two regions that share an interface. The size of each region can be computed as the sum of sizes for each Voronoi cell, and the size of the interface is the sum of the sizes for each segment that comprises it. The Voronoi diagram and the convex hull of each Voronoi cell (volume and boundary) can be computed using the publicly available software package `qhull` or any of the algorithms in O'Rourke [40].

these segments completely and thus define a closed region. This region, known as a Voronoi cell, is always convex and it is possible to determine its size (area).

Now suppose that the points are separated into two groups: the open circles and the closed circles, as in Fig. 21*C*. Then only some of the segments (solid lines) will separate the two groups, while the others will not (dashed lines). In this example, the points represented by a closed circle form a group that defines a closed region of space that consists of the union of the Voronoi cells of each of the points. This larger region (Fig. 21*D*) is no longer convex, but its size (area) can be computed by adding the sizes of the Voronoi cells. In addition, the size of the boundary of the region can be computed by adding the lengths of the segments that comprise it. Note that this procedure can be used to define any region of space, i.e. a shape, by using more points.

**Algorithm 2** ComputeSetup. The calculation of the Voronoi diagram as well as of the volume of the convex hull of a set of points is documented in O'Rourke [40]. The freely available software package `qhull` contains efficient implementations for both.

```
1: INPUT: Groups of points G_1, ..., G_k, of which G_1 is the bounding group; diffusion coefficient D
2: OUTPUT: Geometry of k − 1 cells CSegs, size S(i), production function ρ(i), interface size
   I(i, j), diffusion matrix M(i, j)
3: { vsegs, vcells } ← Voronoi(∪_{i=1}^{k} G_i)
4: for i = 2 to k do
5:     S(i) ← 0
6:     for all P ∈ G_i do
7:         S(i) ← S(i)+ConvexHullVolume(vcells(P))
8:     end for
9:     CSegs(i − 1) ← ComputeBoundarySegs(G_i, vsegs, vcells) {See Algorithm 3}
10: end for
11: for i = 1 to k − 1 do
12:     for j = 1 to k − 1 and j ≠ i do
13:         I(i, j) ← ComputeIntersectionLength(G_i, G_j, vcells) { See Algorithm 4}
14:         M(i, j) ← D ∗ I(i, j)
15:     end for
16: end for
17: for i = 1 to k − 1 do
18:     M(i, i) ← Σ_{j≠i} −M(i, j)
19:     ρ(i) ← 1/S(i)
20: end for
```

**Algorithm 3** ComputeBoundarySegs($G, vsegs, vcells$).

```
1: INPUT: A group of points G, Voronoi segments vsegs, Voronoi cells vcells
2: OUTPUT: Segments segs that form the boundary of G with other groups.
3: segs ← ∅
4: for seg ∈ vsegs do
5:     if P ∈ G, Q ∉ G s.t. seg ∈ vcell(P) and seg ∈ vcell(Q) then
6:         segs ← segs ∪ {seg}
7:     end if
8: end for
```

**Algorithm 4** ComputeIntersectionLength($G_i, G_j, vcells$).

```
1: INPUT: A group of points G, Voronoi segments vsegs, Voronoi cells vcells
2: OUTPUT: Length of intersection len.
3: len ← 0
4: for seg ∈ vsegs do
5:     if P ∈ G_i, Q ∈ G_j s.t. seg ∈ vcell(P) and seg ∈ vcell(Q) then
6:         len ← len+Length(seg)
7:     end if
8: end for
```

Now suppose that there are three groups of points as in Fig. 21*E*: open circles, closed circles, and closed diamonds. This configuration defines two closed regions of space (Fig. 21*F*) which share some of the Voronoi segments (dashed line). As before, the size of each region can be determined and the size of the interface between the two region can be computed as well. Thus, this method can not only define any shape but it can also provide both the shape size (area) and the size of the interface between any two neighboring shapes. These were the requirements for a collection of plant cells.

Fig. 22 shows how this procedure is used to compute the geometry and topology of a traced root. The original image is of the root cell structure in a slice of the *Arabidopsis* root hand-traced by an expert. In Fig. 22*B*, we determine those pixels that belong to the interior of cells and color them white. Pixels with other colors separate different cells but are otherwise not used in the computation. We draw a bounding white curve around the root the pixels of which correspond to the points denoted by open circles in Fig. 21. We extract the coordinates of each white pixel and group the resulting points by computing the contiguous regions of white pixels. Thus, each cell interior is represented by a different (but unique) group of points and the bounding white curve is the only additional group. Then we follow the procedure above and obtain the shapes of each cell as well as their sizes and interfaces. The bounding curve is necessary in order to make sure that all Voronoi cells inside plant cells are finite regions of space.

This same procedure works in higher dimensions as well. For example, the Voronoi diagram of points in three dimensions can be computed efficiently and three dimensional shapes (representing plant cell) can be obtained exactly similarly. The notion of cell size then becomes volume, and interface size becomes area. Both of these can be computed using the values from Voronoi cells as in the two-dimensional case discussed above. Thus, this approach produces the required graph structure for three-dimensional cell measurements as well.

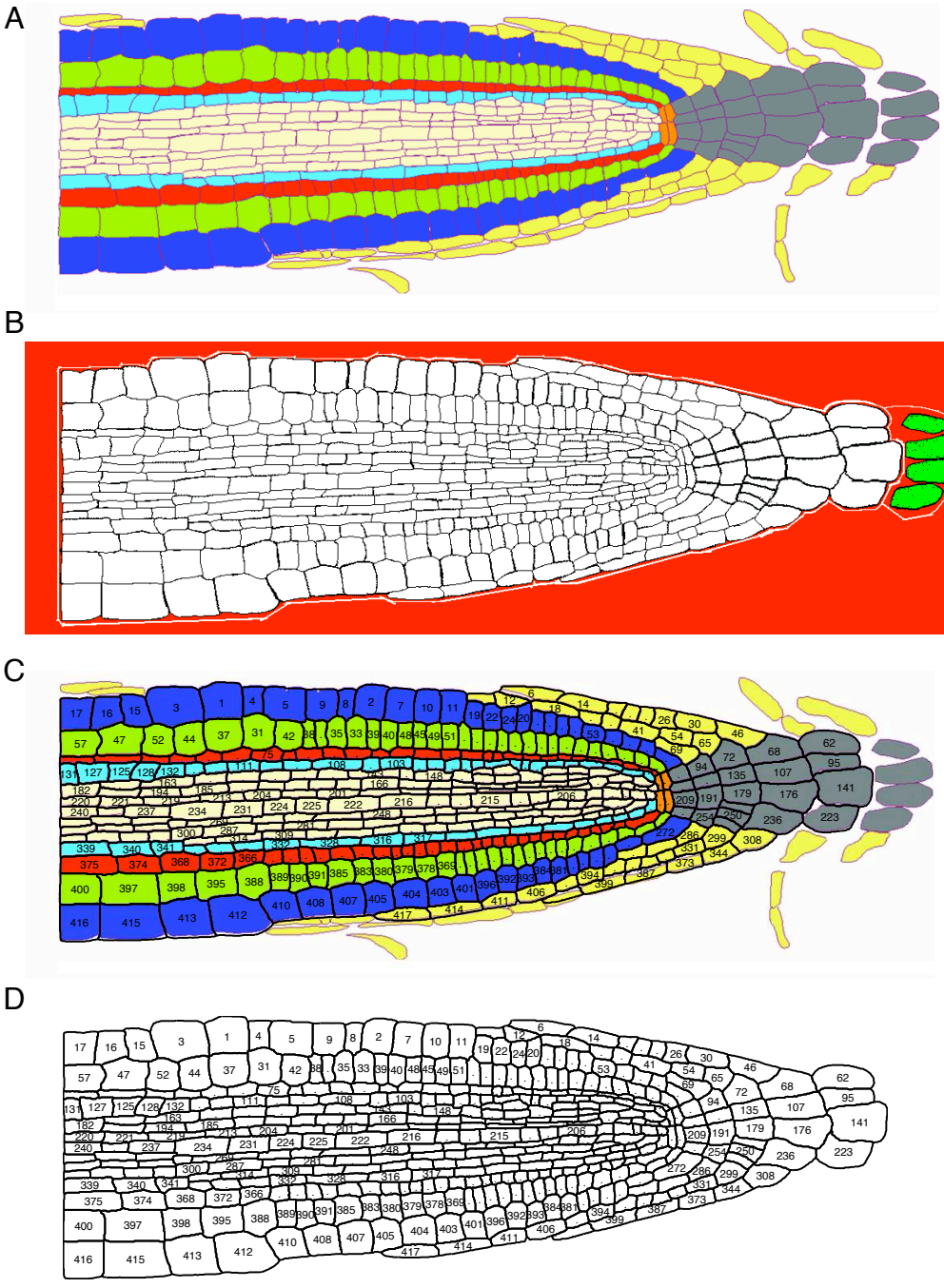


Figure 22: Extracting the geometry and topology of a traced the root slice. **(A)** Image of a hand-traced root slice by an expert. **(B)** Processed image. White pixels in the interior of cells, other colors for display purposes and to separated different cells. **(C)** Result of procedure overlaid on top of original image. **(D)** Result of procedure. All cells are numbered but a dot "." is displayed for small cells.

# References


[1] L. Abas, R. Benjamins, N. Malenica, T. Paciorek, and J. Wisniewska. Intracellular trafficking and proteolysis of the *arabidopsis* auxin-efflux facilitator PIN2 are involved in root gravitropism. *Nat. Cell Biol.*, 8:249, 2006.

[2] R. B. Alan Marchant, I. Casimiro, J. Eklöf, P. J. Casero, M. Bennett, and G. Sandberg. Aux1 promotes lateral root formation by facilitating indole-3-acetic acid distribution between sink and source tissues in the arabidopsis seedling. *Plant Cell*, 14:589–597, 2002.

[3] U. Alon. *An Introduction to Systsems Biology: Design Principles of Biological Circuits*. Mathematical and Computational Biology Series. Chapman & Hall / CRC Press, 2007.

[4] R. C. Bean, W. C. Shepherd, and H. Chan. Permeability of lipid bilayer membranes to organic solutes. *The Journal of General Physiology*, 52:495–508, 1968.

[5] E. Benková, M. Michniewicz, M. Sauer, T. Teichmann, D. Seifertová, G. Jürgens, and J. Friml. Local, efflux-dependent auxin gradients as a common module for plant organ formation. *Cell*, 115(5):591–602, 2003.

[6] M. J. Bennett, A. Marchant, H. G. Green, S. T. May, and W. S. P. Arabidopsis aux1 gene: a permease-like regulator of root gravitropism. *Science*, 273:948, 1996.

[7] J. J. Blakeslee, W. A. Peer, and A. S. Murphy. Auxin transport. *Current Opinion in Plant Biology*, 8:494–500, 2005.

[8] I. Blilou, J. Xu, M. Wildwater, V. Willemsen, I. Paponov, J. Friml, R. Heidstra, M. Aida, K. Palme, and B. Scheres. The PIN auxin efflux facilitator network controls growth and patterning in *arabidopsis* roots. *Nature*, 433:39–44, 2005.

[9] N. Briggs. *Algebraic Graph Theory*. Cambridge University Press, 2 edition, 1993.

[10] D. E. Brown, A. M. Rashotte, A. S. Murphy, J. Normanly, and T. B. W. Flavonoids act as negative regulators of auxin transport in vivo in arabidopsis. *Plant Physiol.*, 126:524, 2001.

[11] T. B. S. Chatfield. Embryogenesis: Pattern formation from a single cell. In C. R. Somerville and E. M. Meyerowitz, editors, *The Arabidopsis Book*. American Society of Plant Biologists, 2002.

[12] R. Chen, P. Hilson, J. Sedbrook, E. Rosen, T. Caspar, and P. H. Masson. The *arabidopsis thaliana* AGRAVITROPIC 1 gene encodes a component of the polar-auxin-transport efflux carrier. *Proc. Natl. Acad. Sci. USA*, 95:15112, 1998.

[13] S. Dharmasiri, R. Swarup, K. Mockaitis, N. Dharmasiri, S. K. Singh, M. Kowalchyk, A. Marchant, S. Mills, G. Sandberg, M. J. Bennett, and M. Estelle. Axr4 is required for localization of the auxin influx facilitator aux1. *Science*, 312(5777):1218–1220, 2006.

[14] P. Dimitrov and S. W. Zucker. Patterns in plant development #1: Uniform production and proportional destruction of auxin. submitted to PLoS.

[15] P. Dimitrov and S. W. Zucker. Patterns in plant development #3: Early pin patterning and shoot-root synchronization. submitted to PLoS.

[16] P. Dimitrov and S. W. Zucker. A *constant production hypothesis* that predicts the dynamics of leaf venation patterning. *Proc. Natl. Acad. Sci USA*, 103:9363–9368, 2006.

[17] M. Eigen. Kinetics of reaction control and information transfer in enzymes and nucleic acids. In S. Claesson, editor, *Proc. Nobel Symp. 5th*, pages 333–369. Almqvist and Wiksell, Stockholm, Swed., 1967.

[18] J. Friml, E. Benkova, I. Blilou, J. Wisniewska, and T. Hamann. AtPIN4 mediates sink-driven auxin gradients and root patterning in *arabidopsis*. *Cell*, 108:661, 2002.

[19] J. Friml and K. Palme. Polar auxin transport—old questions and new concepts? *Plant Molecular Biology*, 49:273–284, 2002.

[20] J. Friml, A. Vieten, M. Sauer, D. Weijers, and H. Schwarz. Efflux-dependent auxin gradients establish the apical-basal axis of *arabidopsis*. *Nature*, 426:147, 2003.

[21] J. Friml, J. Wisniewska, E. Benkova, K. Mendgen, and K. Palme. Lateral relocation of auxin efflux regulator PIN3 mediates tropism in *arabidopsis*. *Nature*, 415:806, 2002.

[22] L. Galweiler, C. Guan, A. Muller, E. Wisman, and K. Mendgen. Regulation of polar auxin transport by atpin1 in arabidopsis vascular tissue. *Science*, 282:2226, 1998.

[23] H. G. Garcia, J. Kondev, N. Orme, J. A. Theriot, and R. Phillips. A first exposure to statistical mechanics for life scientists. arXiv:0708.1899v1.

[24] P. Gil, E. Dewey, J. Friml, Y. Zhao, and K. C. Snowden. BIG: a calossin-like protein required for polar auxin transport in arabidopsis. *Genes Dev.*, 15:1985, 2001.

[25] A. Goldbeter and J. Daniel E. Koshland. An amplified sensitivity arising from covalent modification in biological systems. *Proc. Natl. Acad Sci. USA*, 78:6840–6844, 1981.

[26] M. H. M. Goldsmith. The polar transport of auxin. *Annual Review of Plant Physiology*, 28:439–478, 1977.

[27] M. H. M. Goldsmith, T. H. Goldsmith, and M. H. Martin. Mathematical analysis of the chemosmotic polar diffusion of auxin through plant tissues. *Proc. Natl. Acad Sci. USA*, 78:976–980, 1981.

[28] J. Gutknecht and D. C. Tosteson. Diffusion of weak acids across lipid bilayer membranes: Effects of chemical reactions in the unstirred layers. *Science*, 182:1258–1261, 1973.

[29] J. Gutknecht and A. Walter. Transport of auxin (indoleacetic acid) through lipid bilayer membranes. *Journal of Membrane Biology*, 56:65–72, 1980.

[30] I. D. Kerr and M. J. Bennett. New insight into the biochemical mechanisms regulating auxin transport in plants. *Biochem. J.*, 401:613–622, 2007.

[31] W. J. Lucas and J.-Y. Lee. Plasmodesmata as a supracellular control network in plants. *Nature Reviews Molecular Cell Biology*, 5:712–726, 2004.

[32] C. Luschnig, R. A. Gaxiola, P. Grisafi, and G. R. Fink. EIR1, a root-specific protein involved in auxin transport, is required for gravitropism in *arabidopsis thaliana*. *Genes Dev.*, 12:2175, 1998.

[33] J. Monod, J. Wyman, and J.-P. Changeux. On the nature of allosteric transitions: A plausible model. *J Mol Biol*, 12:88–118, 1965.

[34] A. Muller, C. Guan, L. Galweiler, P. Tanzler, and P. Huijser. AtPIN2 defines a locus of *arabidopsis* for root gravitropism control. *EMBO J.*, 17:6903, 1998.

[35] A. Murphy, W. A. Peer, and L. Taiz. Regulation of auxin transport by aminopeptidases and endogenous flavonoids. *Planta*, 211:315, 2000.

[36] A. S. Murphy, K. R. Hoogner, W. A. Peer, and L. Taiz. Identification, purification, and molecular cloning of N-1-naphthylphthalmic acid-binding plasma membrane-associated aminopeptidases from arabidopsis. *Plant Physiol.*, 128:935, 2002.

[37] B. Noh, A. Bandyopadhyay, W. A. Peer, E. P. Spalding, and M. A. S. Enhanced gravi- and phototropism in plant mdr mutants mislocalizing the auxin efflux protein PIN1. *Nature*, 424:999, 2003.

[38] B. Noh, A. S. Murphy, and S. E. P. Multidrug resistance-like genes of arabidopsis required for auxin transport and auxin-mediated development. *Plant Cell*, 13:2441, 2001.

[39] K. Okada, J. Ueda, M. K. Komaki, C. J. Bell, and Y. Shimura. Requirement of the auxin polar transport system in early stages of arabidopsis floral bud formation. *Plant Cell*, 3:677, 1991.

[40] J. O'Rourke. *Computational Geometry in C*. Cambridge University Press, second edition, 1998.

[41] T. Paciorek, E. Zamalová, N. Ruthardt, J. Petráek, J. K.-V. York-Dieter Stierhof1, D. A. Morris, N. Emans, G. Jürgens, N. Geldner, and J. Friml. Auxin inhibits endocytosis and promotes its own efflux from cells. *Nature*, 435:1251–1256, 2005.

[42] J. Petrásek, J. Mravec, R. Bouchard, J. J. Blakeslee, M. Abas, D. Seifertová, J. Wisniewska, Z. Tadele, M. Kubes, M. Covanová, P. Dhonukshe, P. Skupa, E. Benková, L. Perry, P. Krecek, O. R. Lee, G. R. Fink, M. Geisler, A. S. Murphy, C. Luschnig, E. Zazímalová, and J. Friml. PIN proteins perform a rate-limiting function in cellular auxin efflux. *Science*, 312:914–918, 2006.

[43] M. Ptashne. *A Genetic Switch: Phage Lambda Revisited*. CSHL Press, 2004.

[44] J. A. Raven. Transport of indoleacetic acid in plant cells in relation to ph and electrical potential gradients, and its significance for polar iaa transport. *New Phytologist*, 74:163–172, 1975.

[45] D. Reinhardt, E.-R. Pesce, P. Stieger, T. Mandel, K. Baltensperger, M. Bennett, J. Traas, J. Friml, and C. Kuhlemeier. Regulation of phyllotaxis by polar auxin transport. *Nature*, 426:255–260, 2003.

[46] P. Rubery and A. Sheldrake. Effect of ph and surface charge on cell uptake of auxin. *Nature New Biology*, 244:285–288, 1973.

[47] P. H. Rubery and A. R. Sheldrake. Carrier-mediated auxin transport. *Planta*, 118:101–121, 1974.

[48] S. Sabatini, D. Beis, H. Wolkenfelt, J. Murfett, T. Guilfoyle, J. Malamy, P. Benfey, O. Leyser, N. Bechtold, P. Weisbeek, and B. Scheres. An auxin-dependent distal organizer of pattern and polarity in the arabidopsis root. *Cell*, 99:463–472, 1999.

[49] T. Sachs. The control of patterned differentiation of vascular tissues. *Advances in Botanical Research*, 9:151–262, 1981.

[50] D. Santelia, V. Vincenzetti, E. Azzarello, L. Bovet, Y. Fukao, P. Düchtig, S. Mancuso, E. Martinoia, and M. Geisler. Mdr-like abc transporter atpgp4 is involved in auxin-mediated lateral root and root hair development. *FEBS Letters*, 579:5399–5406, 2005.

[51] E. Scarpella, P. Francis, and T. Berleth. Stage-specific markers define early steps of procambium development in arabidopsisleaves and correlate termination of vein formation with mesophyll differentiation. *Development*, 131:3445–3455, 2004.

[52] E. Scarpella, D. Marcos, J. Friml, and T. Berleth. Control of leaf vascular patterning by polar auxin transport. *Genes and Development*, 20(8):1015–1027, 2006.

[53] O. Serralbo, J. M. Perez-Perez, R. Heidstra, and B. Scheres. Non-cell-autonomous rescue of anaphase-promoting complex function revealed by mosaic analysis of HOBBIT, an Arabidopsis CDC27 homolog. *Proceedings of the National Academy of Sciences*, 103(35):13250–13255, 2006.

[54] T. Sieberer, G. J. Seifert, M. T. Hauser, P. Grisafi, G. R. Fink, and C. Luschnig. Post-transcriptional control of the arabidopsis auxin efflux carrier EIR1 requires AXR1. *Curr. Biol.*, 10:1595, 2000.

[55] R. Swarup, J. Friml, A. Marchant, K. Ljung, G. Sandberg, K. Palme, and M. Bennett. Localization of the auxin permease aux1 suggests two functionally distinct hormone transport pathways operate in the arabidopsis root apex. *Genes and Developlment*, 15:2648–2653, 2001.

[56] R. Swarup, J. Kargul, A. Marchant, D. Zadik, A. Rahman, R. Mills, A. Yemm, S. T. a. I. M. Sean May a Lorraine Williams Paul Millnere, R. Napier, I. D. Kerrg, and M. J. Bennett. Structure-function analysis of the presumptive arabidopsis auxin permease aux1. *The Plant Cell*, 16:3069–3083, 2004.

[57] K. Utsuno, T. Shikanai, Y. Yamada, and T. Hashimoto. Agr, an agravitropic locus of *arabidopsis thaliana*, encodes a novel membrane-protein family member. *Plant Cell Physiol.*, 39:1111, 1998.

[58] A. Vieten, M. Sauer, P. B. Brewer, and J. Friml. Molecular and cellular aspects of auxin-transport-mediated development. *Trends in Plant Science*, 7:160–168, 2007.

[59] A. Vieten, S. Vanneste, J. Wisniewska, E. Benkova, R. Benjamins, T. Beeckman, C. Luschnig, and J. Friml. Functional redundancy of PIN proteins is accompanied by auxin-dependent cross-regulation of PIN expression. *Development*, 132(20):4521–4531, 2005.

[60] Y. Yang, U. Z. Hammes, C. G. Taylor, D. P. Schachtman, and E. Nielsen. High-affinity auxin transport by the aux1 influx carrier protein. *Current Biology*, 16(11):1123–1127, 2006.